

**A GLOBAL REANALYSIS OF NUCLEAR
PARTON DISTRIBUTION FUNCTIONS**K.J. Eskola^{a,b,1}, V.J. Kolhinen^{a,b,2}, H. Paukkunen^{a,b,3} and C.A. Salgado^{c,4,5}^a*Department of Physics, P.O. Box 35, FI-40014 University of Jyväskylä, Finland*^b*Helsinki Institute of Physics, P.O. Box 64, FI-00014 University of Helsinki, Finland*^c*Dipartimento di Fisica, Università di Roma “La Sapienza” and INFN, Roma, Italy***Abstract**

We determine the nuclear modifications of parton distribution functions of bound protons at scales $Q^2 \geq 1.69 \text{ GeV}^2$ and momentum fractions $10^{-5} \leq x \leq 1$ in a global analysis which utilizes nuclear hard process data, sum rules and leading-order DGLAP scale evolution. The main improvements over our earlier work *EKS98* are the automated χ^2 minimization, simplified and better controllable fit functions, and most importantly, the possibility for error estimates. The resulting 16-parameter fit to the $N = 514$ datapoints is good, $\chi^2/\text{d.o.f} = 0.82$. Within the error estimates obtained, the old *EKS98* parametrization is found to be fully consistent with the present analysis, with no essential difference in terms of χ^2 either. We also determine separate uncertainty bands for the nuclear gluon and sea quark modifications in the large- x region where they are not stringently constrained by the available data. Comparison with other global analyses is shown and uncertainties demonstrated. Finally, we show that RHIC-BRAHMS data for inclusive hadron production in d+Au collisions lend support for a stronger gluon shadowing at $x < 0.01$ and also that fairly large changes in the gluon modifications do not rapidly deteriorate the goodness of the overall fits, as long as the initial gluon modifications in the region $x \sim 0.02 - 0.04$ remain small.

¹kari.eskola@phys.jyu.fi²vesa.kolhinen@phys.jyu.fi³hannu.paukkunen@phys.jyu.fi⁴carlos.salgado@cern.ch⁵Permanent address: Departamento de Física de Partículas, Universidade de Santiago de Compostela, Spain

1 Introduction

Universal, process-independent parton distribution functions (PDFs) of free and bound nucleons are a key element in the computational phenomenology of processes involving large virtualities Q^2 in hadronic and nuclear collisions. The free proton PDFs are nowadays rather well constrained through the global analyses [1, 2, 3], which use the DGLAP [4] Q^2 -evolution, sum rules and a large amount of data from deep inelastic lepton–proton scattering (DIS) and high energy proton–(anti)proton collisions. The success of the forthcoming Large Hadron Collider (LHC) program in the search for the Higgs boson and physics beyond the Standard Model depends on the precision of the PDFs.

At collider energies, hard processes are abundantly available also in heavy–ion collisions. These processes play an important role in testing QCD dynamics and factorization, as well as in the search of quark-gluon plasma signatures and in the determination of the QCD matter properties. Similar to the free proton case, the computation of nuclear hard process cross sections requires the nuclear parton distributions (nPDFs) as input. Thus, there is an obvious need for the global analyses of the nPDFs such as presented in [5, 6, 7, 8, 9].

Hard partonic processes taking place at mid-rapidities in nuclear collisions at the Relativistic Heavy Ion Collider (RHIC; $A+A$ and $d+Au$ at $\sqrt{s_{NN}} = 200$ GeV) typically probe the nPDFs in a kinematic region where the nuclear effects remain relatively small and are fairly well constrained by the global analyses. Towards smaller scales and off mid-rapidity, however, the probed region extends towards smaller momentum fractions x where both the nuclear effects and the uncertainties in the nPDFs grow larger. Soon at the Large Hadron Collider (LHC; $Pb+Pb$ at $\sqrt{s_{NN}} = 5.5$ TeV) the range of scales and fractional momenta probed will be widened further, both towards smaller x and towards larger Q^2 . This, together with the fact that the nuclear gluon distributions are still relatively badly known, emphasizes the importance and topicality of the global analyses in pinning down the nPDFs and their uncertainties.

The fact that nuclear and free proton PDFs are mutually different has been known for well over twenty years; for a recent review, see Ref. [10]. The nuclear effects, the nuclear modifications relative to the free proton PDFs, are usually named according to the observed behaviour of the nucleus-to-Deuterium ratio of the structure functions F_2^A in different x -regions, as follows: (i) shadowing; a depletion at $x \lesssim 0.1$, (ii) antishadowing; an excess at $0.1 \lesssim x \lesssim 0.3$, (iii) EMC effect; a depletion at $0.3 \lesssim x \lesssim 0.7$ and (iv) Fermi motion; an excess towards $x \rightarrow 1$ and beyond. This nomenclature will be used in this paper as well. The dynamical origin of these nuclear modifications has been actively studied in different frameworks as well, see the Refs. e.g. in [10, 11, 12]. The DGLAP evolution of the nPDFs and their modifications relative to the free proton PDFs have been studied for two decades, see e.g. Refs. [14, 15, 16, 17, 18, 19, 20, 21, 12].

In a global DGLAP analysis the nPDFs are pinned down as model-independently as possible at a chosen initial scale on the basis of DGLAP evolution, sum rules and hard process data from nuclear collisions. So far, three groups have presented global

DGLAP analyses of the nPDFs analogous to those of the free proton. These are the ones by us, Eskola *et al.* *EKS98* [5, 6], by Hirai *et al.* *HKM* [7] and *HKN* [8], and by de Florian and Sassot *nDS* [9]. The *EKS98* analysis [5, 6] was the first one to show that a good overall fit to the nuclear DIS and Drell-Yan (DY) data can be obtained in a DGLAP-based global analysis. In particular, the scale-dependence of the ratio $F_2^{\text{Sn}}/F_2^{\text{C}}$ observed by the NMC experiment [13] was very nicely reproduced by tuning the initial gluon modifications suitably. The iterative χ^2 minimization in *EKS98* was carried out manually (by eye), and no well-controlled error estimates were obtained. Since then, extensive further work has been done by Kumano and his collaborators in estimating these uncertainties [7, 8], and by de Florian and Sassot [9] in bringing the global nPDF analysis to the next-to-leading order (NLO) level.

In this paper, we perform a global analysis of the nPDFs in the *EKS98* framework. Our study is partly a reanalysis of *EKS98* as we take some guidelines from this old fit. To minimize the number of fit parameters, however, we now apply simpler piecewise analytical shapes for the nuclear effects at the initial scale. We also construct the nuclear quark modifications in a more transparent way than in our previous work. The goal here is twofold: on one hand, by making the χ^2 minimization procedure automated, we wish to check whether the goodness of the old *EKS98* fit could still be improved, and on the other hand we wish to get a better hold on the uncertainties of the nPDFs, of the gluons in particular, in this framework.

The results of this study can be summarized as follows: Within the obtained χ^2 and error estimates, we conclude that the old *EKS98* parametrization still serves very well. Thus, we do not release a new parametrization but recommend to use *EKS98*. We also demonstrate how the small- x nuclear gluon distributions are, in spite of the good overall fit obtained, still not well constrained with the currently available nuclear DIS and DY data elsewhere than perhaps at $x \sim 0.02 - 0.04$. A comparison with the results from the previous global analyses is also shown, demonstrating the nPDFs uncertainties concretely. Finally, a special case beyond the original *EKS98* setup, a gluon shadowing clearly stronger than that in F_2^A/F_2^D , is considered and further developments of the analysis by inclusion of RHIC data are discussed.

This paper is organized as follows. In Sec. 2, we define nPDFs according to the *EKS98* framework and introduce the fitting procedure. Section 3 contains the results of χ^2 minimization and the a detailed comparison with the nuclear DIS and DY data. Section 4 is devoted for the comparison with previous global analyses. In Sec. 5 we show the results from the error analysis performed and verify the validity of *EKS98*. In Sec. 6, we discuss the possibility of a stronger gluon shadowing supported by the RHIC data. Conclusions and further discussion are given in Sec. 7.

2 The framework

2.1 Definition of nPDFs

As introduced in *EKS98* [5], by a nuclear parton distribution function f_i^A we refer to the distribution of a parton type i in a proton¹ bound to a nucleus of a mass number A . We define and parametrize the nuclear modifications relative to the known free proton PDFs f_i ,

$$R_i^A(x, Q^2) = \frac{f_i^A(x, Q^2)}{f_i(x, Q^2)}. \quad (1)$$

In the *EKS98* framework which we adopt here, the PDFs of the bound neutrons are obtained from $f_i^A(x, Q^2)$ by assuming isospin symmetry. Thus, e.g. the total u -quark distribution in a nucleus of a mass number A and a proton number Z becomes $U_A = Zf_u^A + (A - Z)f_d^A$. Correspondingly, the lowest-order QCD parton model expression for the lA DIS structure function F_2 then becomes $F_2^A = \sum_Q e_Q^2 [Q_A + \overline{Q}_A]$, where $Q = U, D, S, \dots$

The total amount of fit parameters in the initial ratios R_i^A must be limited for obtaining converging well-constrained fits. Unfortunately, the variety of the nuclear data is presently not enough to pin down each $R_i^A(x, Q_0^2)$ separately. Therefore, following the *EKS98* procedure, we can include only three different ratios for each nucleus at an initial scale $Q^2 = Q_0^2$ where heavy quarks can be neglected: The same average modification $R_V^A = (f_{uv}^A + f_{dv}^A)/(f_{uv} + f_{dv})$ is applied for all valence quarks separately (only at Q_0^2 however), the corresponding sea quark average modification R_S^A applied for all sea quarks separately (again at Q_0^2 only) and R_G^A for gluons. While this is the best we can do here, we note that the valence u and d quark nuclear modifications may in fact well differ from each other – for a recent study of how large differences between R_{uv}^A and R_{dv}^A would explain the NuTeV weak-mixing angle anomaly observed in $\nu(\bar{\nu}) + \text{Fe}$ DIS, see [23]. Also, in the sea quark sector, due to their mutually differing absolute distributions, it would be natural to expect that the initial s quark modifications are not necessarily identical to those of u and d . Without a multitude of further data constraints, however, such details cannot be reliably included in a global analysis.

In the original *EKS98* analysis [5] we first parametrized the DIS structure function ratio

$$R_{F_2}^A(x, Q^2) \equiv \frac{\frac{1}{A}F_2^A(x, Q^2)}{\frac{1}{2}F_2^D(x, Q^2)} \quad (2)$$

at the initial scale Q_0^2 and then decomposed this into the valence and sea parts. The initial gluon modifications were obtained by adding a double gaussian distribution on the antishadowing peak of the parametrized $R_{F_2}^A$. In the current analysis we choose a more straightforward procedure by parametrizing directly the ratios R_V^A , R_S^A and R_G^A at Q_0^2 .

¹Note that in *HKN* a slightly different definition is used, see [7, 8].

The initial scale is here chosen to be $Q_0 = 1.3$ GeV in order to match the CTEQ6L1 PDF set [3], which we use to calculate the absolute nuclear PDFs at Q_0^2 :

$$f_i^A(x, Q_0^2) = R_i^A(x, Q_0^2) f_i^{\text{CTEQ6L1}}(x, Q_0^2). \quad (3)$$

The lowest order DGLAP scale evolution is calculated using the routine from the CTEQ collaboration [22] as it provided fast enough evolution for the minimization purposes.

The key constraints for the nPDFs are given by the nuclear hard process data from lepton-nucleus DIS and from the DY dilepton production in proton-nucleus collisions. We utilize the results from the DIS measurements, available in the form of ratios over Deuterium and Carbon,

$$\frac{\frac{1}{A} d\sigma^{lA}/dQ^2 dx}{\frac{1}{2} d\sigma^{lD}/dQ^2 dx} \stackrel{\text{LO}}{=} R_{F_2}^A(x, Q^2), \quad \frac{\frac{1}{A} d\sigma^{lA}/dQ^2 dx}{\frac{1}{12} d\sigma^{lC}/dQ^2 dx} \stackrel{\text{LO}}{=} \frac{R_{F_2}^A(x, Q^2)}{R_{F_2}^C(x, Q^2)}, \quad (4)$$

where the LO connection is implied. The DY data are available in the form of ratios over Deuterium and Beryllium,

$$\frac{\frac{1}{A} d\sigma_{DY}^{\text{pA}}/dx_2 dQ^2}{\frac{1}{2} d\sigma_{DY}^{\text{pD}}/dx_2 dQ^2} \stackrel{\text{LO}}{=} R_{DY}^A(x_2, Q^2), \quad \frac{\frac{1}{A} d\sigma_{DY}^{\text{pA}}/dx_1 dQ^2}{\frac{1}{9} d\sigma_{DY}^{\text{pBe}}/dx_1 dQ^2} \stackrel{\text{LO}}{=} \frac{R_{DY}^A(x_1, Q^2)}{R_{DY}^{\text{Be}}(x_1, Q^2)}. \quad (5)$$

Above, Q^2 is the invariant mass of the dilepton pair and $Q^2 = x_1 x_2 \sqrt{s_{NN}}$. The data included in this study are shown in Table 1. The small nuclear effects in Deuterium are neglected.

As will become clear in the error analysis presented in Sec. 5, the available sets of experimental data do not constrain the distributions of different parton flavours over the whole range of x . This will be reflected as some assumptions regarding the shape of the ratios which are basically the same as in our previous *EKS98* work. In particular, motivated by the requirement of a stable evolution (that the nuclear modifications should not change very rapidly from their starting values), a saturation (flattening) of the ratios R_i^A at $x \rightarrow 0$, and a valence quark -like behavior of the sea and gluon modifications for $x \rightarrow 1$ will be assumed. In the following we explain in detail how the initial parametrization for $R_V^A(x, Q_0^2)$, $R_S^A(x, Q_0^2)$ and $R_G^A(x, Q_0^2)$ was constructed.

2.2 Fit functions and parameters

While the basic idea in the global DGLAP analysis is straightforward, it is a surprisingly nontrivial task to develop functional forms for the fit functions for the ratios R_V^A , R_S^A and R_G^A which can be used in the automated χ^2 minimization process in a transparent way. To have a better control over the multidimensional parameter space and over the numerical results obtained, each parameter should preferably have a clear interpretation, too. Due to the various A and x dependent nuclear effects discussed above and also due to the mutual differences between the valence, sea and gluon modifications, the fit functions must contain sufficiently many parameters to secure enough

Experiment	Process	Nuclei	datapoints	Ref.
SLAC E-139	DIS	He(4)/D	18	[25]
NMC 95, reanalysis	DIS	He/D	16	[27]
SLAC E-139	DIS	Be(9)/D	17	[25]
NMC 96	DIS	Be(9)/C	15	[29]
SLAC E-139	DIS	C(12)/D	7	[25]
NMC 95	DIS	C/D	15	[28]
FNAL-E665	DIS	C/D	4	[26]
NMC 95, reanalysis	DIS	C/D	16	[27]
FNAL-E772	DY	C/D	9	[24]
SLAC E-139	DIS	Al(27)/D	17	[25]
NMC 96	DIS	Al/C	15	[29]
SLAC E-139	DIS	Ca(40)/D	7	[25]
FNAL-E665	DIS	Ca/D	4	[26]
FNAL-E772	DY	Ca/D	9	[24]
NMC 95, reanalysis	DIS	Ca/D	15	[27]
NMC 96	DIS	Ca/C	15	[29]
SLAC E-139	DIS	Fe(56)/D	23	[25]
FNAL-E772	DY	Fe/D	9	[24]
NMC 96	DIS	Fe/C	15	[29]
FNAL-E866	DY	Fe/Be	28	[30]
SLAC E-139	DIS	Ag(108)/D	7	[25]
NMC 96, Q^2 dep.	DIS	Sn(117)/C	144	[13]
FNAL-E772	DY	W(184)/D	9	[24]
FNAL-E866	DY	W/Be	28	[30]
SLAC E-139	DIS	Au(197)/D	18	[25]
FNAL-E665	DIS	Pb(208)/D	4	[26]
NMC 96	DIS	Pb/C	15	[29]
FNAL-E665	DIS, recal.	Pb/C	4	[26]
total number of datapoints			514	

Table 1: The data used in this analysis, grouped according to the nuclei measured. The mass numbers are given in parentheses. The number of datapoints refers to those falling into the region $Q^2 \geq Q_0^2$.

flexibility necessary for obtaining good fits. At the same time, the number of parameters has to be reduced to a minimum in order to obtain converging fits with the rather limited set of data constraints at our disposal. Finally, once the working functional forms have been verified, one needs to analyze (on the basis of the data constraints and χ^2 fits) which parameters can be left free and which can be fixed. Furthermore, the best local minimum in χ^2 has to be verified by optimizing the the initial values of all free parameters. All this implies extensive manual labour, even though the actual search for the χ^2 minimum is automated.

For the controllability discussed above, and after various other attempts, we ended up constructing each of the initial ratios R_V^A , R_S^A and R_G^A from three different pieces: $R_1^A(x)$ at small values of x below the antishadowing² maximum, $x \leq x_a^A$; $R_2^A(x)$ in the medium- x region from the antishadowing maximum to the EMC minimum, $x_a^A \leq x \leq x_e^A$; and $R_3^A(x)$ in the Fermi-motion region in the large- x region, $x \geq x_e^A$;

$$R_1^A(x) = c_0^A + (c_1^A + c_2^A x)[\exp(-x/x_s^A) - \exp(-x_a^A/x_s^A)], \quad x \leq x_a^A \quad (6)$$

$$R_2^A(x) = a_0^A + a_1^A x + a_2^A x^2 + a_3^A x^3, \quad x_a^A \leq x \leq x_e^A \quad (7)$$

$$R_3^A(x) = \frac{b_0^A - b_1^A x}{(1-x)^{\beta^A}}, \quad x_e^A \leq x. \quad (8)$$

In choosing the above forms, we were motivated by the functional forms used before in Hard Probes [31] (see [32]), *EKS98* [5] and *HKN* [8]. Matching is done by requiring continuity of the fit functions and setting their first derivatives to zero at x_a^A (local maximum) and x_e^A (local minimum). As the coefficients a_i^A , b_i^A and c_i^A are somewhat unintuitive, we shall quote the results in terms of the following more transparent set of seven parameters from which these coefficients can be easily solved:

y_0^A	R_1^A at $x \rightarrow 0$,
x_s^A	a slope factor in the exponential,
x_a^A, y_a^A	position and height of the antishadowing maximum
x_e^A, y_e^A	position and height of the EMC minimum
β^A	slope of the divergence of R_3 at $x \rightarrow 1$.

Each of the above parameters is in principle yet specific to a nucleus A . This (at least) doubles the amount of parameters. We parametrize the A -dependence in a simple power-like form:

$$z_i^A = z_i^{A_{\text{ref}}} \left(\frac{A}{A_{\text{ref}}} \right)^{p_{z_i}}, \quad (9)$$

where $z_i = x_s, x_a, y_a \dots$, and choose the reference nucleus to be Carbon, $A_{\text{ref}} = 12$. The number of parameters we have for the valence, sea and gluon ratios each is thus 14: the Carbon parameters (suppressing the superscript C to lighten the notation) y_0 , x_s , x_a , x_e , y_a , y_e , β , and their powers p_{y_0} , p_{x_s} , p_{x_a} , p_{x_e} , p_{y_a} , p_{y_e} and p_β . Altogether this makes $3 \times 14 = 42$ free parameters. Even if the momentum and baryon number

²For antiquarks $R_S^A < 1$, by antishadowing we refer to the shape similar to $R_{F_2}^A$.

conservation, imposed individually for each nucleus, reduce this number by four, it is clearly far too large for a converging χ^2 minimization process, given the limited data constraints we have. In order to radically reduce the number of free parameters, we proceed as follows, keeping in mind the focus on the small- and medium- x regions.

- Fermi-motion. In the large- x region, where valence quarks dominate, the DIS or DY data do not give proper constraints for gluons or sea quarks. Thus, we fix the Fermi-motion slopes β^A in R_S^A and R_G^A to be the same as in R_V^A . Based on our previous *EKS98* work, we fix $\beta = 0.3$ and $p_\beta = 0$ in R_V^A , thus ignoring a possible A -dependence of β^A .
- EMC effect. Gluons originate from valence quarks at small scales and large x . Therefore, they should reflect the EMC effect observed in R_V^A ($R_{F_2}^A$). From the gluons the effect should then be transmitted on to R_S^A as well. We have checked that this is indeed the case in the DGLAP evolution [33]. Thus, by assuming the similarity of the EMC-minima in each initial ratio R_G^A , R_S^A and R_V^A , one reaches a stable scale evolution of this nuclear effect. As the available data, however, constrain the EMC effect in detail only in R_V^A , we fix the location parameters x_e^A and the magnitude parameters y_a^A of the EMC-minima in R_G^A and R_S^A to be identical to those in R_V^A . For the valence part, we noticed that allowing for an A dependence in x_e^A did not improve the overall fits, hence we fix $p_{x_e} = 0$ for simplicity.
- Antishadowing. In course of the present analysis we also noticed that the location parameters x_a^A of the antishadowing maxima in R_V^A and in R_S^A typically become almost A -independent and that the weak A dependence does not improve the obtained fits. We therefore set $p_{x_a} = 0$ in R_V^A and R_S^A . In order to reduce the number of gluon parameters to the very minimum, we simply fix x_a^A of gluons to be identical to that in valence but leave y_a and p_{y_A} free for controlling the height of the antishadowing maximum in an A -dependent way.
- Shadowing. In the small- x parts, based on χ^2 -checks, we drop the A -dependence of the slope parameters x_s^A , hence setting p_{x_s} to zero and leaving x_s free in all ratios.
- Conservation laws. Baryon number and momentum conservation are used to calculate y_0^A for R_V^A and R_G^A , respectively, for each nucleus individually. This eliminates the parameters y_0 and p_{y_0} for the valence and gluon modifications. For the sea quarks, these parameters are left free.

All this brings the number of free parameters down to 16: $x_s, x_a, x_e, y_a, p_{y_a}, y_e$ and p_{y_e} in R_V^A ; $y_0, p_{y_0}, x_s, x_a, y_a$ and p_{y_a} in R_S^A ; and $x_s, y_a,$ and p_{y_a} in R_G^A . Table 2 summarizes the above discussion on the parameters as well as their values obtained in

finding a "best" local minimum with respect to the fit parameters for

$$\chi^2 = \sum_{i=1}^{N_{\text{data}}} \left(\frac{\text{data}_i - \text{theory}_i}{\Delta_i} \right)^2. \quad (10)$$

As the data errors Δ_i , we take the given statistical and systematic errors added in quadrature.

Some remarks on the functional form adopted for the shadowings at small- x are in order here. Since the valence modification R_V^A is rather well constrained by the DIS and DY data in the large- and medium- x regions, its small- x behaviour becomes relatively stringently constrained by the baryon number sum rule. Unfortunately, in the absence of DIS (or DY) data for $R_{F_2}^A$ at $x < 0.001$ in the DGLAP region $Q^2 \gtrsim 1 \text{ GeV}^2$, the sea quark R_S^A and the gluon R_G^A cannot be pinned down similarly well in the small- x region – thus their behaviour and error estimates at small x are bound to be specific to the fit function forms assumed.

The motivation for choosing the smallest- x form of $R_1^A(x)$ in Eq. (6), where shadowing levels off to a constant value at $x = 0$, is the fact that such saturation of shadowing has been observed in the very small- x & very small- Q^2 DIS data (see Fig. 10 in [28]) and the fact that the Q^2 dependence there is rather weak (see Figs. 11 and 12 in [28]). In doing this, however, we should keep in mind that the implications of the observed saturation of shadowing are not clear for the nPDFs at perturbative scales: power corrections $\sim (Q^2)^{-n}$ [34] are most likely important in the DIS cross sections at small enough scales, and also nonlinearities [35] (neglected here) are expected to play a role in the scale evolution at sufficiently small- x & small- Q^2 .

In the previous *EKS98* analysis, due to the modest and non-negative $\log Q^2$ -slopes of $R_{F_2}^A$ discussed above, we fixed the smallest- x behaviour of $R_{F_2}^A(x, Q_0^2)$ to a value slightly above the saturation of shadowing observed at lower scales. The $\log Q^2$ slopes of $R_{F_2}^A$ computed from the DGLAP equations at small x [36, 5, 32],

$$\frac{\partial R_{F_2}^A(x, Q^2)}{\partial \log Q^2} \propto \alpha_s \frac{xg(2x, Q^2)}{F_2^D(x, Q^2)} \left\{ R_G^A(2x, Q^2) - R_{F_2}^A(x, Q^2) \right\}, \quad (11)$$

are non-negative if $R_G^A(2x) \geq R_{F_2}^A(x)$. In *EKS98*, it was shown that an ansatz $R_G^A(x \rightarrow 0) \rightarrow R_{F_2}^A(x \rightarrow 0)$ works well for the smallest x . In the present analysis, we want to test the above *EKS98* gluon framework and thus keep the saturation of gluon shadowing independent of that in R_S^A .

3 Results

3.1 Final parameters and their interpretation

In minimizing the χ^2 with respect to the free parameters, we used the MINUIT routines from the CERN Program Library [37]. Only after reducing the number of free parameters down to 16, and after extensive searches for suitable initial parameter values, we

were able to find a converging fit indicating a local minimum of the χ^2 . The obtained parameters for the best fit found are shown in Table 2. The resulting goodness of the fit was $\chi^2 = 410.15$ for $N = 514$ data points and 16 free parameters, giving $\chi^2/N = 0.80$ and $\chi^2/\text{d.o.f.} = 0.82$.

	Param.	Valence	Sea	Gluon
1	y_0	baryon sum	0.88909	momentum sum
2	p_{y_0}	baryon sum	-8.03454×10^{-2}	momentum sum
3	x_s	0.025 (<i>l</i>)	0.100 (<i>u</i>)	0.100 (<i>u</i>)
4	p_{x_s}	0, fixed	0, fixed	0, fixed
5	x_a	0.12190	0.14011	as valence
6	p_{x_a}	0, fixed	0, fixed	0, fixed
7	x_e	0.68716	as valence	as valence
8	p_{x_e}	0, fixed	0, fixed	0, fixed
9	y_a	1.03887	0.97970	1.071 (<i>l</i>)
10	p_{y_a}	1.28120×10^{-2}	-1.28486×10^{-2}	3.150×10^{-2} (<i>u</i>)
11	y_e	0.91050	as valence	as valence
12	p_{y_e}	-2.82553×10^{-2}	as valence	as valence
13	β	0.3	as valence	as valence
14	p_β	0, fixed	as valence	as valence

(*u*) upper limit; (*l*) lower limit

Table 2: List of all parameters defining the modifications R_V^A , R_S^A and R_G^A in Eqs. (6-8) at the initial scale $Q_0^2 = 1.69 \text{ GeV}^2$. The parameters y_0 , y_a , y_e , x_s , x_a , x_e and β are for the reference nucleus $A = 12$, and the powers p_i define the A -dependence in the form of Eq. (9). The obtained final results for the fitted 16 free parameters are shown and the fixed parameters are indicated. The parameters which drifted to their upper (*u*) and lower (*l*) limits are indicated, see the text for details.

As indicated in the table, the parameters x_s controlling the slopes of R_1^A near the antishadowing region were drifting to their limits. In spite of various attempts we failed to improve upon this unwanted feature. Obviously, there is still room for developing the chosen functional forms in the quark sector too. However, as the fits obtained now (and already in *EKS98*) are very good, new functional forms are not likely to improve the χ^2 essentially. In fact, this was our observation also at different stages of the present analysis: in spite of the non-converging fits often obtained (which were due to too many free parameters allowed or badly guessed initial parameter values), the obtained fits themselves were equally good.

The gluon sector, however, is the most troublesome one, as all the data constraints are indirect and not very conclusive when put into the context of a global analysis: rather large changes in the gluon shadowing and antishadowing can be compensated for by fairly moderate modifications in the quark sector. As a result, gluons have a minor effect in the overall χ^2 . The gluonic parameters y_a and p_{y_a} , which are drifting

to their limits (see the table), reflect these problems.

As described above, the functional form R_1^A at very small x preassumes the saturation of shadowing also for gluons. The height of the antishadowing bump y_a and its A -dependence are correlated with the parameters y_0 and its A dependence p_{y_a} which are computed from the momentum sum rule: the larger the y_a , the smaller the y_0 . Even though no essential improvement over the χ^2 was noticed in varying the limits of y_a and p_{y_a} , a clear trend was observed: as indicated by reaching the lower limit of y_a , the amounts of gluon antishadowing and shadowing always tend to be minimized. This in turn means that gluon shadowing saturates at a value larger than that of sea quarks and that the $\log Q^2$ slopes of $R_{F_2}^A$ at the smallest x remain positive. These observations coincide with the results from previous global analyses *HKN* [8] and *nDS* [9].

We thus conclude that the present DIS and DY data and the sum rule constraints suggest that gluon shadowing is weaker or at most as strong as that in sea quarks. As one of the goals here is to test the *EKS98* framework for our final results summarized in Table 2 we have set the lower limits of the free gluonic antishadowing parameters y_a and p_{y_a} in such a way that the gluon shadowing levels off to the same value as that of sea quarks ($R_{F_2}^A$). The benefit in doing this is that we can keep the *EKS98*-like good agreement with the clearly positive $\log Q^2$ slopes of $F_2^{\text{Sn}}/F_2^{\text{C}}$ observed at $x \sim 0.01$, see Fig. 9 ahead.

As explained above, in the present analysis the valence and gluon parameters y_0^A are computed from baryon number and momentum sum rules, correspondingly, for each nucleus separately. For completeness, we note that a power-law fit of Eq. (9) to the values obtained, using $A = 12$ and 208 , gives $y_0 = 0.9288$ and $p_{y_0} = -0.031209$ for valence and $y_0 = 0.8898$ and $p_{y_0} = -0.084315$ for gluons. With such parametrization, baryon number and momentum would be conserved with sufficient accuracy, within a few per cent, for all nuclei.

The obtained initial nuclear modifications are shown in Fig. 1, where we plot $R_V^A(x, Q_0^2)$ (solid lines), $R_S^A(x, Q_0^2)$ (dotted lines), $R_G^A(x, Q_0^2)$ (dashed lines) and $R_{F_2}^A(x, Q_0^2)$ (dotted-dashed lines) for nuclei $A = 12, 40, 117$ and 208 at an initial scale $Q_0^2 = 1.69$ GeV².

The scale evolution of the nuclear effects is shown in Fig. 2, where the ratios are plotted for $A = 12$ and $A = 208$ as a function of x , at fixed scales $Q^2 = Q_0^2 = 1.69$ GeV² (solid), 10 GeV² (dotted) and 10^4 GeV² (dashed). In the regions where no stringent data constraints are available for sea quarks and gluons, notice the systematic scale dependence at small x ($\log Q^2$ slopes do not change their sign), and the stability of the ratios near the EMC minimum.

3.2 Comparison with data

Next we compare the obtained results with the data included in the analysis and illustrate the good overall agreement obtained. The DIS data can be found in Figs. 3-6 and in 9, and the DY data in Figs. 7-8. In the plots below, the statistical and systematic errors of the data have been added in quadrature.

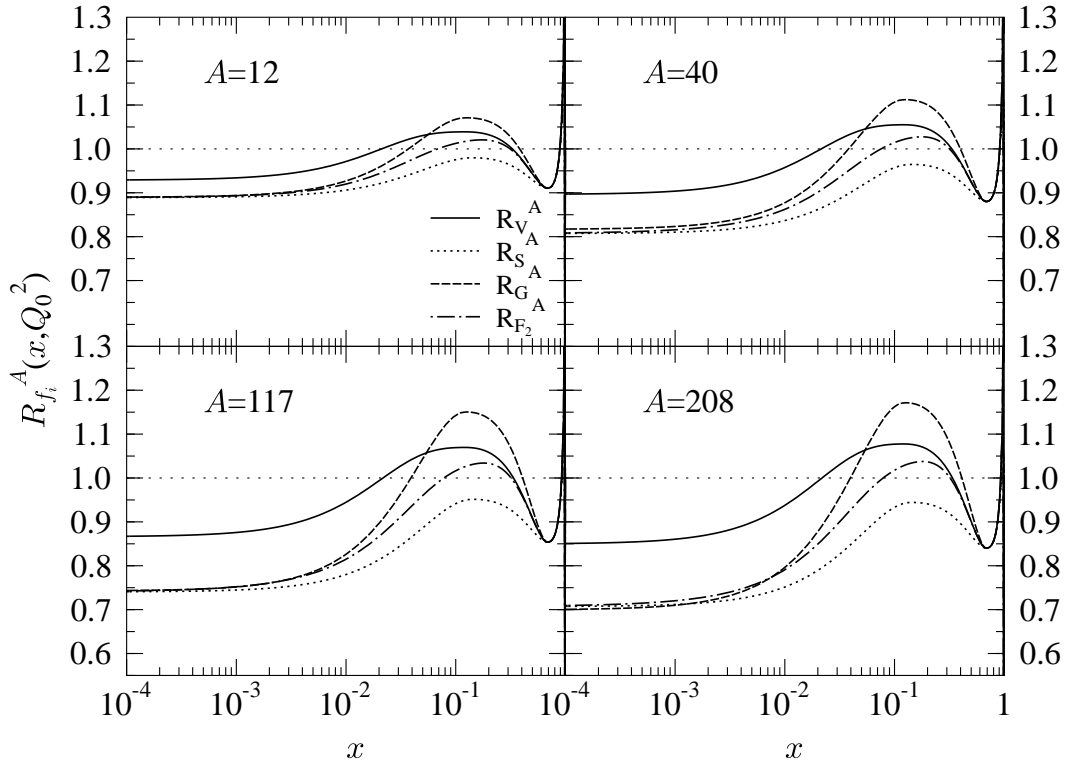


Figure 1: Initial nuclear ratios $R_V^A(x, Q_0^2)$ (solid lines), $R_S^A(x, Q_0^2)$ (dotted lines), $R_G^A(x, Q_0^2)$ (dashed lines) and $R_{F_2}^A(x, Q_0^2)$ (dotted-dashed lines) for $A = 12, 40, 117$ and 208 at $Q_0^2 = 1.69$ GeV^2 .

In Fig. 3 we show the computed ratio $\frac{1}{A}F_2^A/\frac{1}{12}F_2^C = R_{F_2}^A/R_{F_2}^C$ against the NMC data [29] for various nuclei. The open squares are the NMC data points and the filled squares are our results computed at the corresponding values of x and Q^2 . This data set plays a major role in constraining the A -systematics of nuclear quark distributions at small x .

In Fig. 4 we compare the computed ratio $R_{F_2}^A(x, Q^2)$ with the data from SLAC [25], E665 [26], NMC 95 [28] and NMC 95 [27] reanalysis. The open triangles, diamonds, squares and circles stand for the data and the corresponding filled symbols show our results. Note that at the same/similar values of x the values of Q^2 can vary between the different data sets, hence the multiple filled symbols at these x . In the figure, we have also included the small- x data points whose Q^2 -values lie below our initial scale. The asterisks show our results at our Q_0^2 . To compare these points with the data, one should perform the scale evolution downwards. We do not consider this here (and hence these data points are not included in the χ^2 minimization either) but from the figure we can immediately see, as the $\log Q^2$ slopes of $R_{F_2}^A$ are positive and modest, and as the points computed at a higher scale lie above the NMC data, that the agreement is good also in that part of the small- Q^2 region where the DGLAP might still be valid.

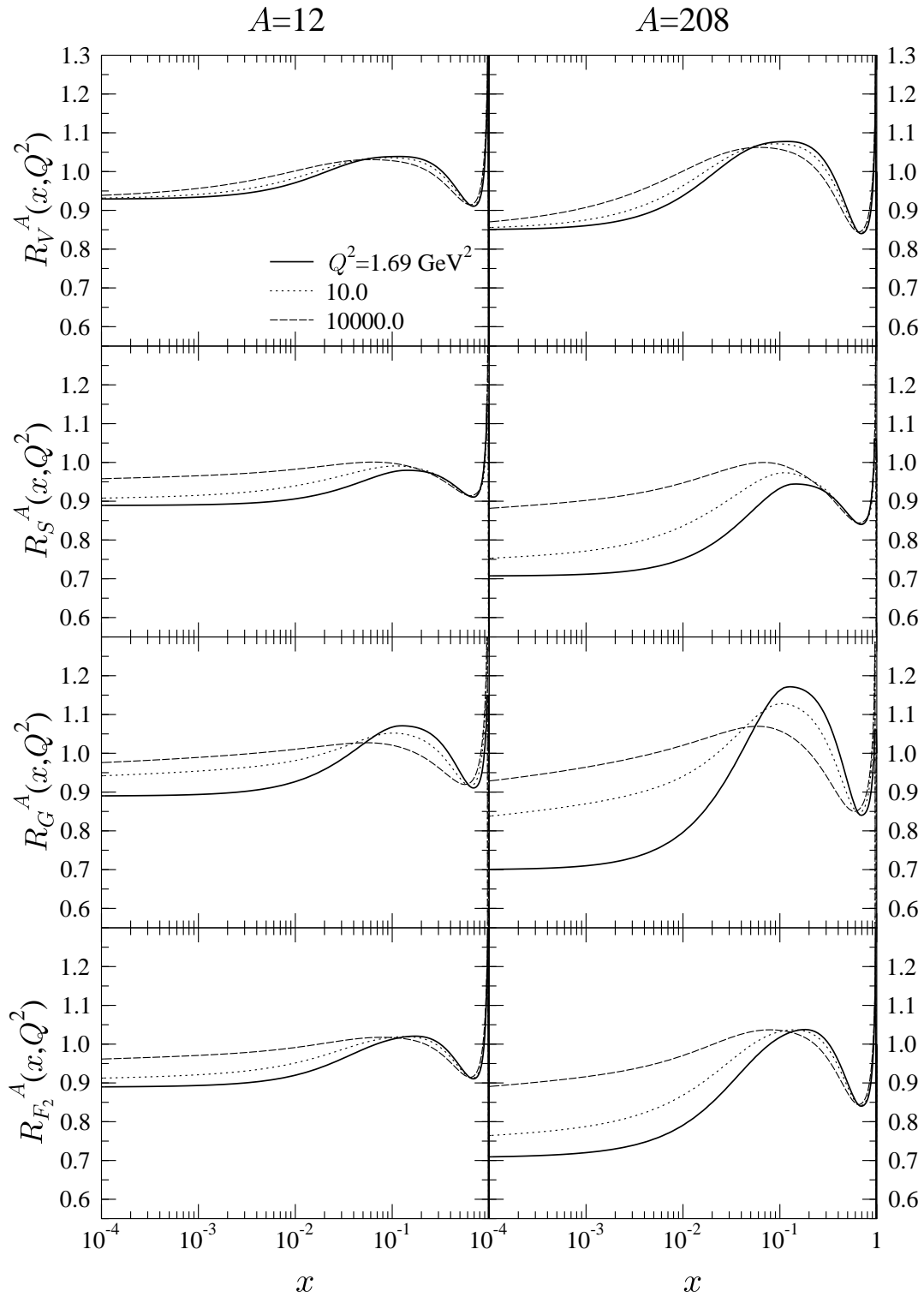


Figure 2: Scale evolution of nuclear modifications: the ratios $R_V^A(x, Q^2)$, $R_S^A(x, Q^2)$, $R_G^A(x, Q^2)$, and $R_{F_2}^A(x, Q^2)$ at scales $Q^2 = 1.69, 100$ and 10000 GeV² for $A = 12$ and 208 .

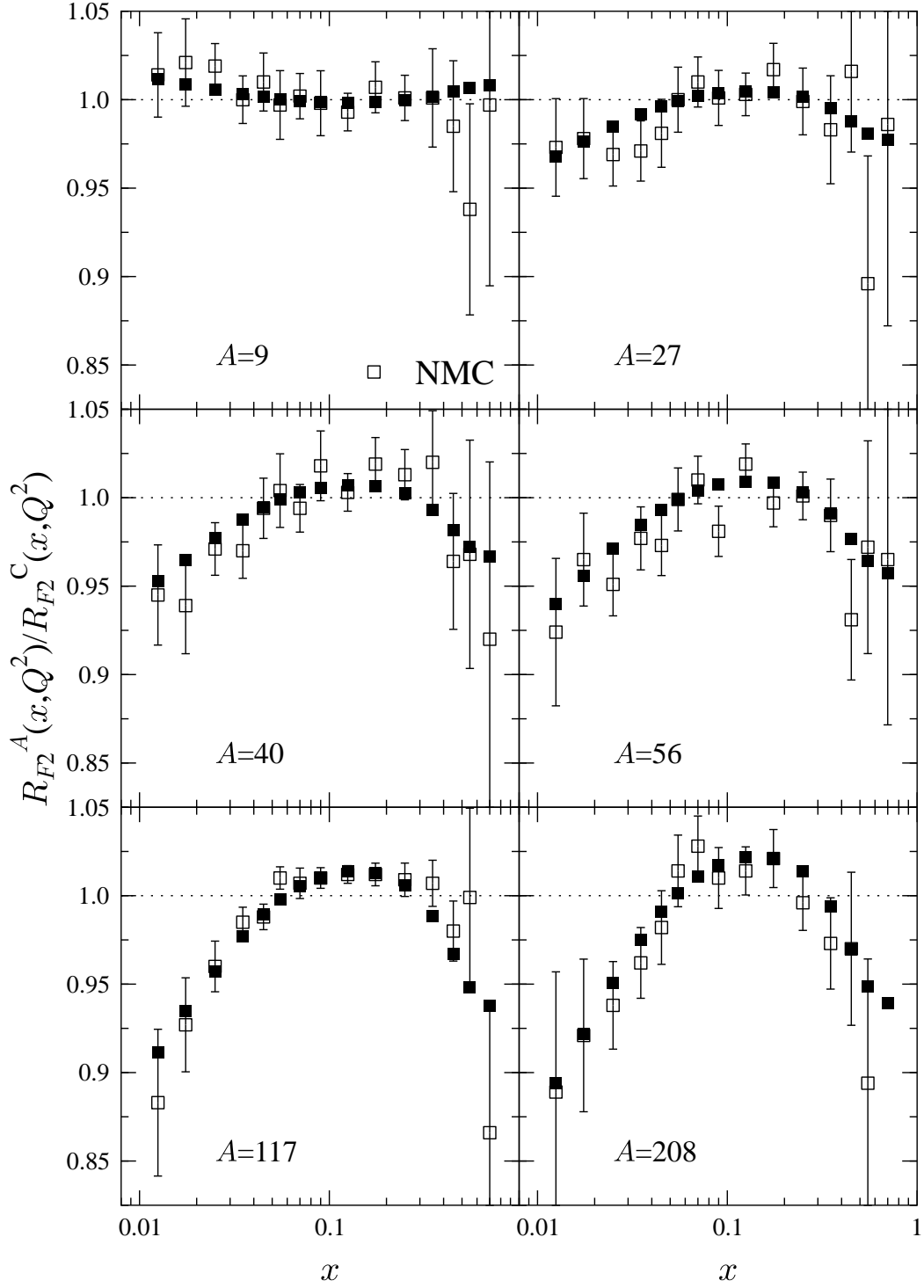


Figure 3: The computed ratio $R_{F_2}^A(x, Q^2)$ vs. $R_{F_2}^C(x, Q^2)$ compared with the NMC data [29]. The open symbols are the data points with errors added in quadrature, the filled ones are the corresponding results from this analysis.

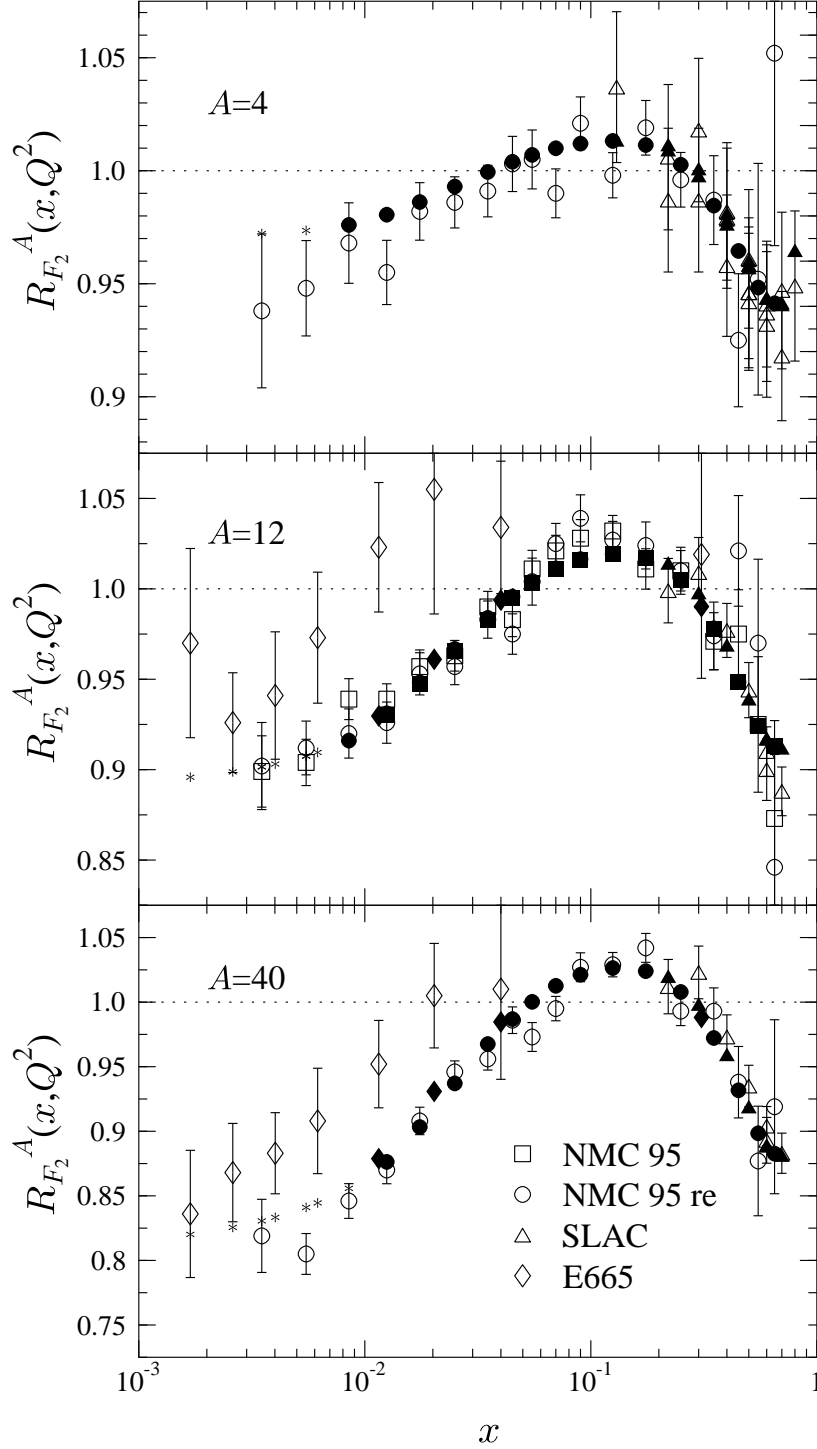


Figure 4: Calculated $R_{F_2}^A(x, Q^2)$ (filled symbols) are compared to SLAC (triangles) [25], E665 (diamonds) [26], NMC 95 (squares) [28] and reanalysed NMC 95 (circles) data [27]. The asterisks denote our results calculated at the initial scale Q_0^2 , these are for the smallest- x data points whose scales lie in the region $Q^2 < Q_0^2$.

Similar comparisons are shown in Fig. 5 for the ratios $R_{F_2}^{\text{Pb}}/R_{F_2}^{\text{D}}$ and $R_{F_2}^{\text{Pb}}/R_{F_2}^{\text{C}}$. In the upper panel we show the ratio $R_{F_2}^{\text{Pb}}/R_{F_2}^{\text{D}}$ from the E665 experiment (open triangles) [26]. The agreement is not very good, which is not surprising as the NMC and E665 data sets in Fig. 4 do not agree, either (the NMC data has more weight in the analysis due to their smaller error bars). However, as noticed by the NMC well in the past [29], if one considers the ratio of ratios, $R_{F_2}^{\text{Pb}}/R_{F_2}^{\text{C}}$, the agreement between these data sets becomes very good. This is shown in the lower panel of Fig. 5, where we plot the data from NMC (open squares) [29] and together with a ratio calculated from the E665 (open triangles) data for $R_{F_2}^{\text{Pb}}$ and $R_{F_2}^{\text{C}}$ [26]. We obtain the error bars for the computed E665 Pb/C ratio by first adding the statistical and systematic errors in quadrature separately for Pb/D and C/D, and then taking these errors to be independent. The filled squares and triangles again show our DGLAP results corresponding to the data points, while the asterisks mark our results at the x -points where our initial scale is higher than the Q^2 in the E665 data.

Further comparison with the SLAC data [25] for $R_{F_2}^A(x, Q^2)$ are shown in Fig. 6 for various nuclei and Q^2 scales. This set of data plays an important role in constraining x - and A -dependence of the valence quark distributions in the EMC region. The filled symbols again stand for our results, the open ones for the data.

Figure 7 shows the comparison of the calculated LO Drell-Yan cross section ratios, Eq. (5), to the FNAL E772 data [24]. The momentum fraction x_2 is that of the nuclear parton. Open squares with error bars present the data points and filled squares show the calculated values. As can be seen, the calculated values fit the data rather well, except at the smallest x_2 -points for tungsten (for which the *EKS98* seems to work slightly better).

Figure 8 then shows the comparison with a newer E866 data set [30] on the DY ratio $(d\sigma^{\text{pA}}/dQ^2 dx_1)/(d\sigma^{\text{pD}}/dQ^2 dx_1)$ as a function of the projectile-parton momentum fraction. Four different invariant mass bins are considered. Large values of x_1 now correspond to small values of x_2 . Confirming the trend seen in the previous figure, we note that the A dependence of shadowing could be slightly stronger in order to better match with the DY data. Within the present global analysis, however, we were unable to improve on this feature.

Finally, in Fig. 9 we plot the scale evolution of the ratio $\frac{1}{117}F_2^{\text{Sn}}/\frac{1}{12}F_2^{\text{C}}$ compared with the data from NMC [13] for several fixed values of x . The $\log Q^2$ slopes of the data at small x , which are sensitive to the gluon modifications as shown in Eq. (11) are reproduced very well, similar to *EKS98*. Note that the 15 panels here correspond to the 15 data points in the lower left panel of Fig. 3, so that the normalization of $\frac{1}{117}F_2^{\text{Sn}}/\frac{1}{12}F_2^{\text{C}}$ at each x is given by the overall fit. Thus in the upper left panel ($x = 0.0125$) of Fig. 9 the normalization is slightly higher than that of the data, while in the third panel ($x = 0.025$) both the normalization and the $\log Q^2$ slopes match perfectly.

The NMC data at the smallest- x panels of Fig. 9 play an important role in constraining the nuclear gluon modifications. These data were the key ingredient in the *EKS98* analysis in pinning down the nuclear gluon modifications around $x \sim 0.03$, for more discussion see also [32]. We note, however, that in an automated global analysis

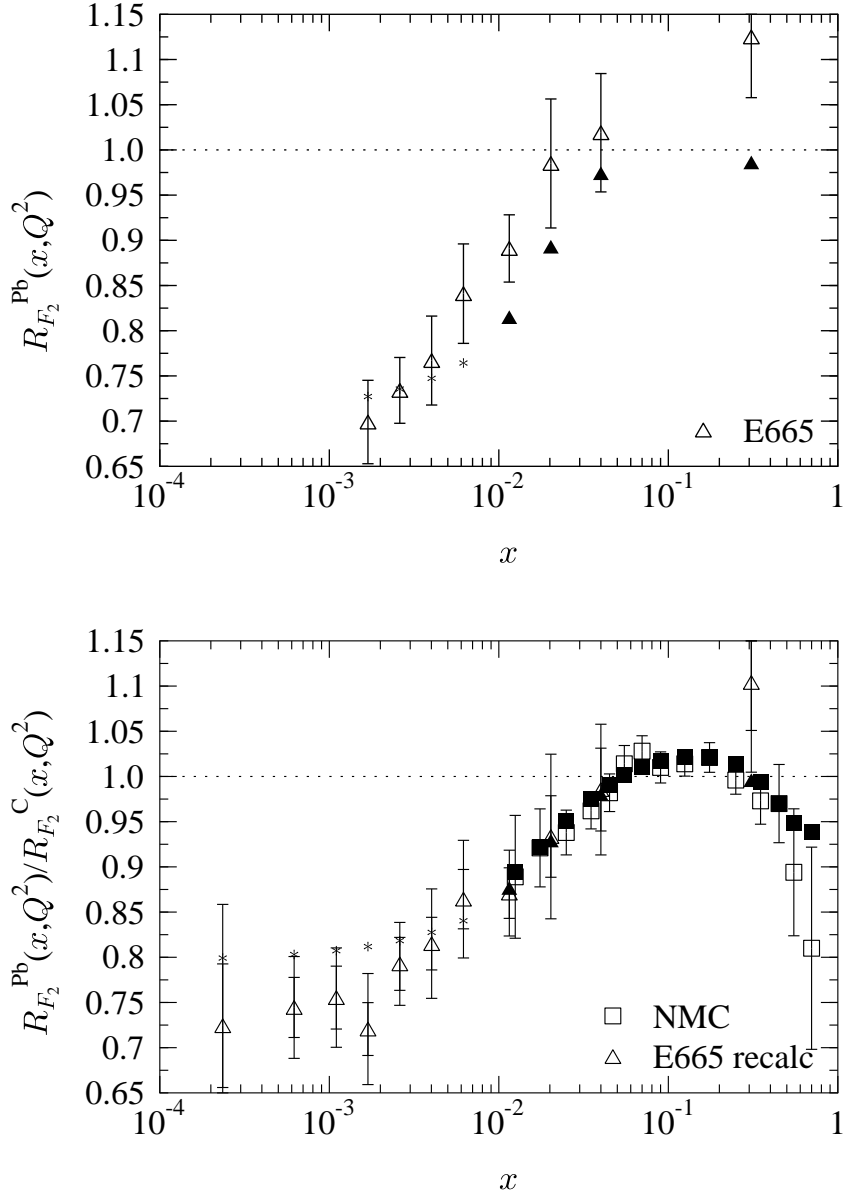


Figure 5: **Top:** The ratios $R_{F_2}^{\text{Pb}}/R_{F_2}^{\text{D}}$ from the E665 experiment (open triangles) [26] compared with the results from the present analysis (filled triangles). **Bottom:** Comparison of the ratios $R_{F_2}^{\text{Pb}}/R_{F_2}^{\text{C}}$. The NMC data [29] are shown by open squares, the ratios calculated from the E665 data [26] by open triangles. For the error estimates in the latter case, see the text. The corresponding theoretical results are again shown by the filled symbols, and by asterisks if the experimental Q^2 is below our initial scale Q_0^2 .

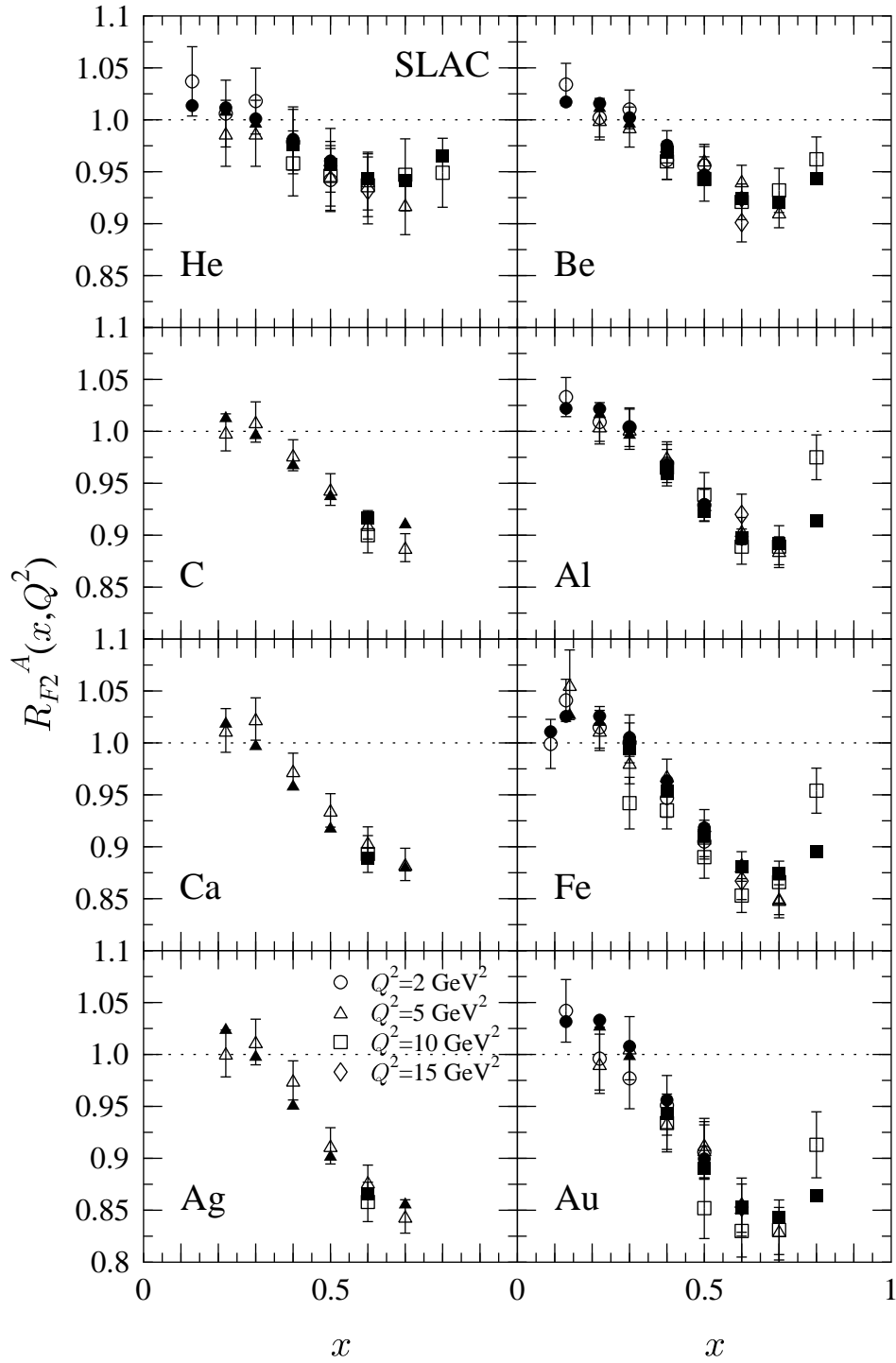


Figure 6: The calculated ratio $R_{F_2}^A(x, Q^2)$ compared with the SLAC data [25]. Data points at $Q^2 = 2 \text{ GeV}^2$ are shown by circles, $Q^2 = 5 \text{ GeV}^2$ by triangles, $Q^2 = 10 \text{ GeV}^2$ by squares and $Q^2 = 15 \text{ GeV}^2$ by diamonds. The corresponding filled symbols mark our results.

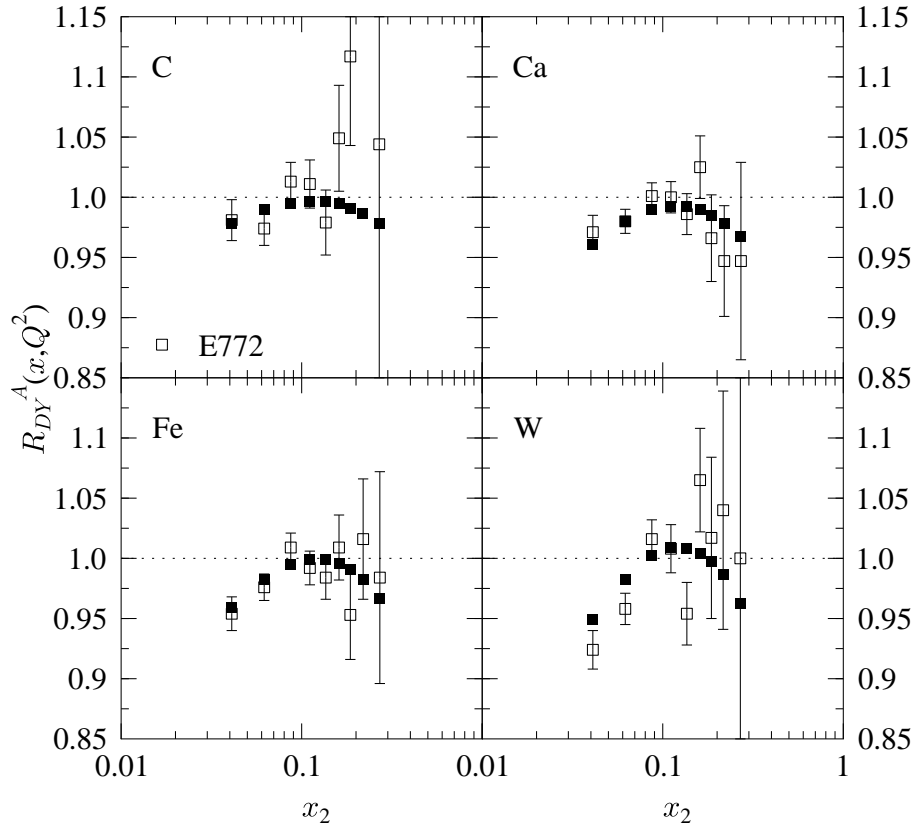


Figure 7: The ratio of the computed LO differential Drell-Yan cross sections (open squares), $(d\sigma^{\text{pA}}/dQ^2 dx_2)/(d\sigma^{\text{pD}}/dQ^2 dx_2)$, and the E772 data [24] (filled squares).

like we perform here, this role becomes not quite as clear: even relatively large variations of the gluon modifications induce changes practically only in the first few panels of this figure. The weight that these these panels have in the χ^2 is rather small among the 500 other data points from cross sections mostly sensitive to the changes in the quark sector.

4 Comparison with previous analyses

Table 3 summarizes the χ^2 obtained in this work, *EKS98* [5, 6], *HKM* [7], *HKN* [8] and *nDS* [9] analyses. Since each analysis uses different initial scales, different amount of data points and different data sets, we quote the values given in the original references (except for *EKS98* whose χ^2 we compute here using CTEQ6L1). As seen in the table, the goodness of the fit using the *EKS98* nuclear effects is very close to the one obtained in this work and also (contrary to the claim in [9]) quite close to the good fit obtained in the LO analysis *nDS*. Interestingly, the χ^2 of the NLO fit of *nDS* is slightly smaller

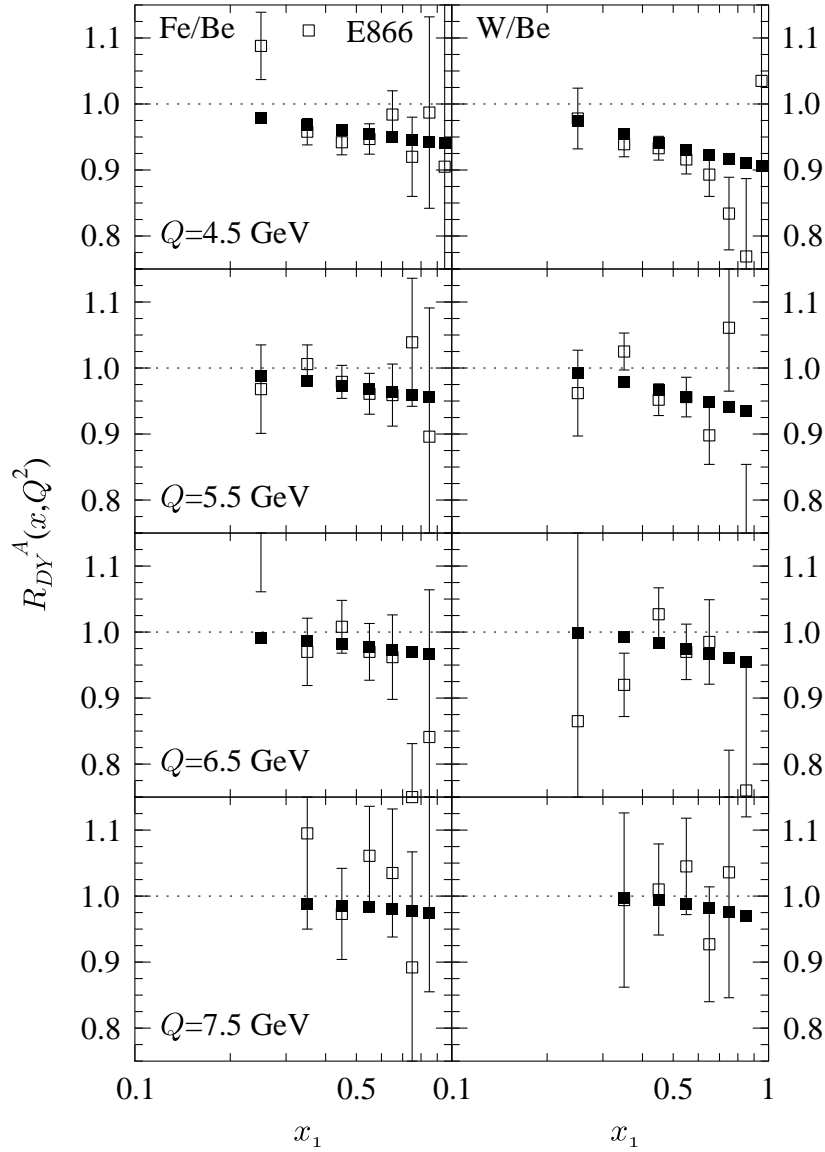


Figure 8: The ratio of the computed LO differential Drell-Yan cross sections (open squares), $(d\sigma^{\text{pA}}/dQ^2 dx_1)/(d\sigma^{\text{pD}}/dQ^2 dx_1)$, compared with the E866 data [30] as a function of x_1 at four different invariant mass (Q^2) bins. Some data points lie outside the shown region; nevertheless their error bars are shown if they extend to the figure.

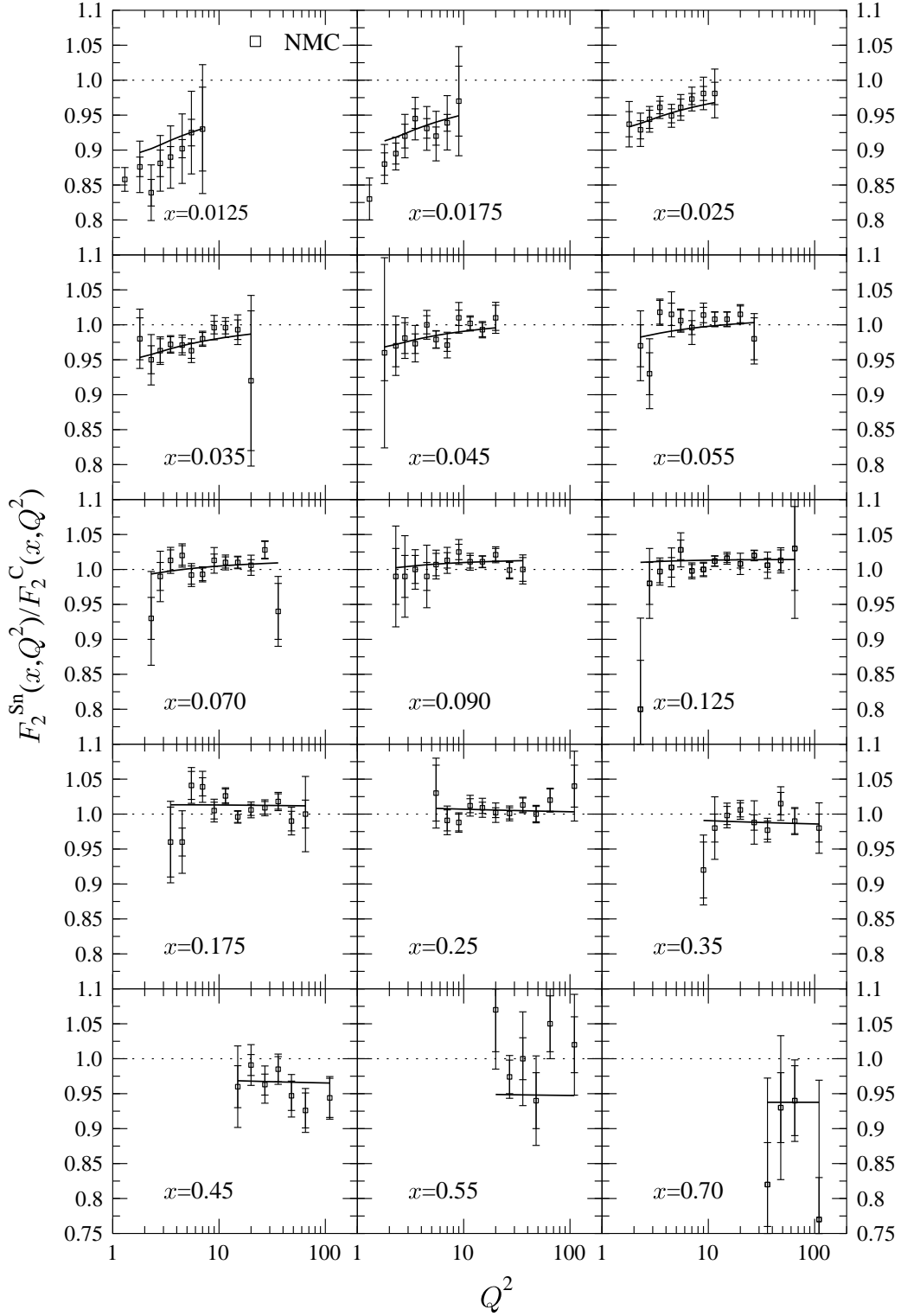


Figure 9: The calculated scale evolution (solid lines) of the ratio $F_2^{\text{Sn}}/F_2^{\text{C}}$ compared with the NMC data [13] for several fixed values of x . The inner error bars are the statistical ones, the outer ones stand for the statistical and systematic errors added in quadrature.

than the LO ones, lending further support to the validity of the global analysis.

Set	Ref.	Q_0^2/GeV^2	N_{data}	N_{params}	χ^2	χ^2/N	$\chi^2/\text{d.o.f.}$
This work		1.69	514	16	410.15	0.798	0.824
<i>EKS98</i>	[5]	2.25	479	–	387.39	0.809	–
<i>HKM</i>	[7]	1.0	309	9	546.6	1.769	1.822
<i>HKN</i>	[8]	1.0	951	9	1489.8	1.567	1.582
<i>nDS</i> , LO	[9]	0.4	420	27	316.35	0.753	0.806
<i>nDS</i> , NLO	[9]	0.4	420	27	300.15	0.715	0.764

Table 3: The goodness of the fits obtained in different global analyses.

To demonstrate the remaining uncertainties in the nPDFs, we show in Fig. 10 the comparison between this work (solid), *EKS98* [5, 6] (dashed), *HKM* [7] (dotted), *HKN* [8] (long-dashed) and *nDS* (NLO) [9] (dot-dashed) sets. The ratios R_V^A , R_u^A , R_G^A and $R_{F_2}^A$ are plotted for $A = 40$ at scales $Q^2 = 2.25$ and 100 GeV^2 . We choose Calcium here as there are both small- x and larger- x DIS data and DY data available for this nucleus. The lower one of the scales considered is the initial scale in the *EKS98* set.

As can be seen in Fig. 10, the quantitative main difference between the present analysis and *EKS98* lies in the small- x behaviour of sea quark and gluon modifications. For the sea quarks, the difference is merely due to the different form of the fit functions chosen: in the present work, shadowing in R_S^A , and thus also that in $R_{F_2}^A$, levels off faster. Like in the original *EKS98* framework, the very-small- x behaviour of R_G^A at Q_0^2 is tied to that of $R_{F_2}^A$ (but indirectly, through restricting the limits of the free parameters controlling the antishadowing maximum), thus also the gluon shadowing saturates now faster than in *EKS98*, and hence we have also somewhat less antishadowing in gluons. Recall also the small difference in the initial scales here and in *EKS98*. In the region $x \sim 0.02 - 0.03$, where the ratios R_G^A are indirectly constrained by the NMC data in Fig. 9, the results from the present work and *EKS98* are very similar.

Regarding all sets, we first notice that in the mid/large- x region $x \gtrsim 0.1$ the ratios $R_{F_2}^A$ are almost identical, thanks to the constraints given by the DIS data for the x , Q^2 and A dependence of $R_{F_2}^A$. Since in the large- x region, $x \gtrsim 0.3$ or so, valence quarks dominate $R_{F_2}^A$, also the ratios R_V^A from different sets agree nicely there.

The role of the DY data in pinning down both R_V^A and R_S^A in the small/mid- x region $0.01 \lesssim x \lesssim 0.3$ can be concretely seen in the figure. In the *HKM* [7] analysis (dotted lines), the DY data was not included. As a result, the *HKM* fit suggested $R_S^A \gg 1$ at $x > 0.1$, which in turn compensated the smallness of $R_V^A(x \sim 0.1)$ (see the left panel) in reproducing $R_{F_2}^A$. The main improvement from *HKM* to *HKN* [8] was the inclusion of the DY data in the fit. This translates into better constraints and a better agreement with *EKS98* for R_V over the whole x -region and also for R_S^A at $0.01 \lesssim x \lesssim 0.1$. The fact that the ratios R_V from different global analyses agree so nicely is quite reassuring, as it demonstrates that the average valence quark modifications can

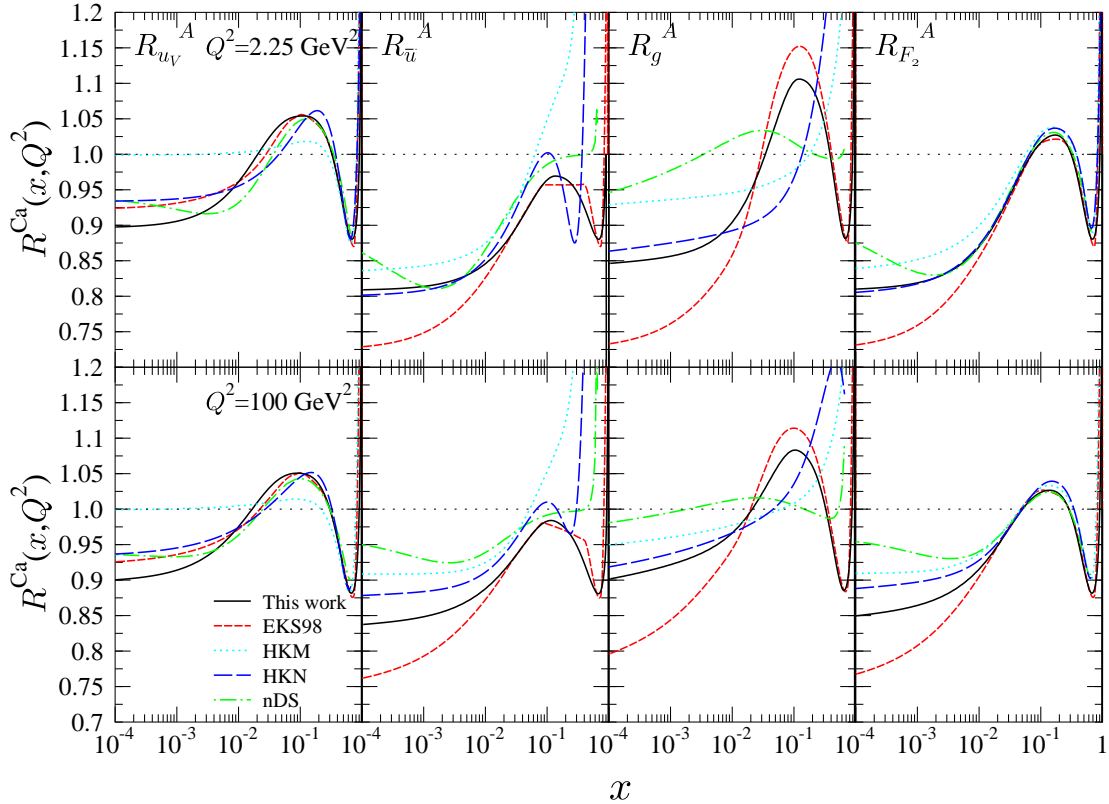


Figure 10: (Colour online) Comparison of different nPDF modifications for Ca: This work, *EKS98* [5, 6], *HKM* [7], *HKN* [8] and *nDS* (NLO) [9] are plotted at scales $Q^2 = 2.25$ and 100 GeV^2 . Calcium is used here as it is fairly well constrained by the data.

be pinned down in a manner which does not depend much on the specific form chosen for the fit functions.

At $x \gtrsim 0.2$, where valence quarks start to dominate the quark sector, sea quarks are not sufficiently constrained by either DIS or DY data – hence the large variations in R_S^A from set to set. This is the case also in the very-small- x region $x \lesssim 0.01$, in the absence of sufficient data constraints there. Thus, the very-small- x behaviour of R_S^A is specific to the form of the fit function chosen.

As can be seen in Fig. 10, the nuclear gluon distributions in general are still quite badly constrained, resulting in large differences between the different sets. In the absence of data which would sufficiently stringently constrain the gluon modifications over a wide enough x -range, the results from the global fits are bound to depend on the form of the fit functions chosen. To demonstrate this, we replot the ratio $\frac{1}{117} F_2^{\text{Sn}} / \frac{1}{12} F_2^{\text{C}}$ in Fig. 11 for the six smallest- x panels of Fig. 9. As can be seen here, the log Q^2 slopes of $F_2^{\text{Sn}} / F_2^{\text{C}}$ become flatter in *HKN* and *HKM* than those in the present analysis, *EKS98* and *nDS*. The reason for this can be seen from the ratios R_G^A at $x \gtrsim 0.02 - 0.04$ in Fig. 10

and from Eq. (11): the larger R_G^A is relative to $R_{F_2}^A$, the faster is the Q^2 dependence of $R_{F_2}^A$. However, as commented in the previous section, the small- x NMC data which would give at least some constraints for the gluons at $x \sim 0.02 - 0.04$, has a relatively small weight in the global analysis. All this makes it difficult to pin down the nuclear gluon modifications.

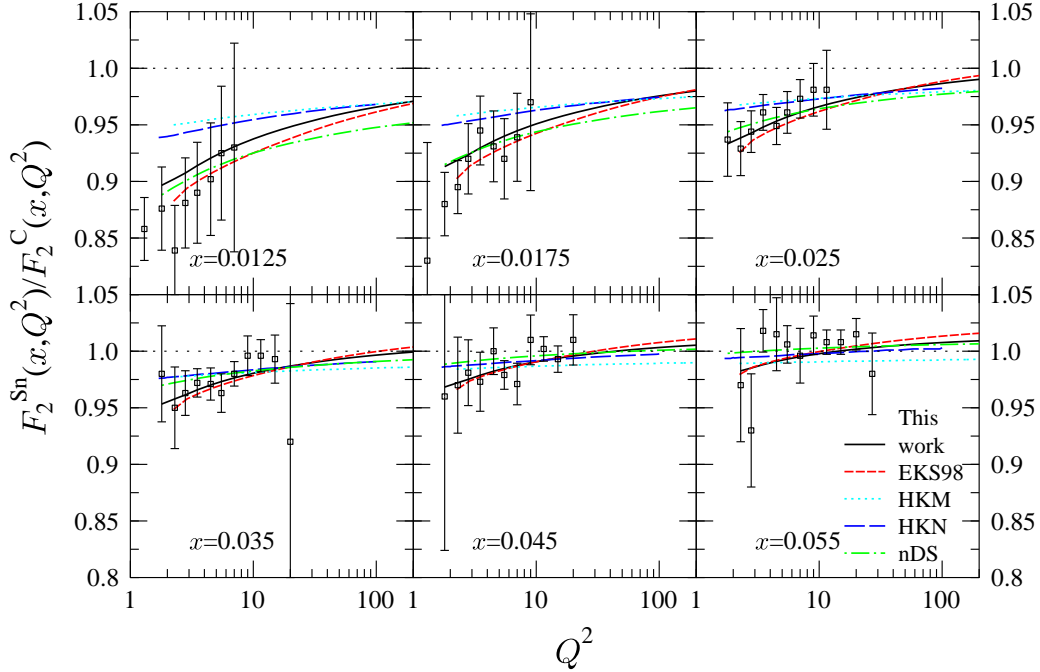


Figure 11: (Colour online) Comparison of the results from this analysis (solid), *EKS98* (dashed), *HKM* (dotted), *HKN* (long-dashed) and *nDS* (dot-dashed) for the ratio $\frac{1}{117}F_2^{\text{Sn}}/\frac{1}{12}F_2^{\text{C}}$. As in Fig. 9 (6 first panels there), the data is from NMC [13].

5 Error Analysis

Next, to quantify the above discussion on the uncertainties, we proceed to the error analysis, one of the goals in the present paper. We do this by using the Hessian method, which is one of the standard methods in multiparameter analyses as it takes the parameter correlation into account. The error matrix, or the Hessian matrix, is the inverse of the second derivative matrix of the fitting function χ^2 with respect to its free parameters. The Minuit fitting routine provides also this matrix along with the fit parameters [37]. Denoting the set of fit parameters by ξ and the Hessian error matrix by H , the fitting function χ^2 can be expanded around the minimum $\hat{\xi}$ as (See e.g. Ref. [38], here we follow the notation of Ref. [39])

$$\Delta\chi^2 = \chi^2(\hat{\xi} + \delta\xi) - \chi^2(\hat{\xi}) = \sum_{i,j} H_{ij}\delta\xi_i\delta\xi_j. \quad (12)$$

The uncertainty of the fitted function $F(x, \hat{\xi})$ is then

$$[\delta F(x, \hat{\xi})]^2 = \Delta\chi^2 \sum_{i,j} \left(\frac{\partial F(x, \hat{\xi})}{\partial \xi_i} \right) H_{ij}^{-1} \left(\frac{\partial F(x, \hat{\xi})}{\partial \xi_j} \right), \quad (13)$$

assuming linear error propagation. However, the confidence region of a multivariable fit is different than that of a single variable fit and needs to be evaluated. The confidence level P of the normal distribution with N degrees of freedom can be written as

$$P = \int_0^{\Delta\chi^2} \frac{1}{2\Gamma(\frac{N}{2})} \left(\frac{S}{2} \right)^{\frac{N}{2}-1} \exp\left(-\frac{S}{2}\right) dS, \quad (14)$$

where $\Gamma(n)$ is the Gamma function. For one-parameter fit the one- σ error range results confidence level $P = 0.6826$ and $\Delta\chi^2 = 1$. Requiring the same confidence level for N parameters one can now calculate the $\Delta\chi^2$. For example, for $N = 16$ one obtains $\Delta\chi^2 = 18.11$.

The error limits obtained using this method for the fit with the 16 free parameters in Table 2 are shown by the dashed lines in Fig. 12 for the ratios R_V^A , R_S^A , R_G^A and $R_{F_2}^A$ in the case of a Lead nucleus, $A = 208$. As can be seen from Fig. 12, and as expected on the basis of Sec. 4, the ratio R_V^A is relatively well constrained. Also $R_{F_2}^A$ is rather well under control. At large x its errors naturally follow the small errors of R_V^A , thanks to the DIS data available. In the small/mid- x region both the DIS data and the DY data are necessary to pin down R_V^A and R_S^A . Towards smaller values of x the errors in R_S^A get larger due to the lack of high-precision constraints for the sea quarks there, but are nevertheless still constrained. As discussed in Sec. 4, the small- x errors of R_S^A shown, and thereby those in $R_{F_2}^A$, are specific to the small- x behaviour assumed. Hence, the error bars given here are to be considered as lower limits.

For the gluons, the very-small- x errors become quite large as there are no data constraints there to guide us. Similarly to the sea quark case, the error bars on gluon shadowing are fit function specific, and hence lower limits. However, as noticed in *EKS98* and originally in Ref. [40] gluons do get somewhat better constrained at $x \sim 0.02 - 0.04$, thanks to the NMC data. Note that the zero-error we obtain at the peak of the gluon antishadowing bump is an artifact due to the interplay between the free parameters and the momentum sum rule.

To get physically more relevant estimates on the sea quark and gluon uncertainties for the mid- and large- x regions, we do the following. We free the parameters y_a , p_{y_a} , y_e , p_{y_e} and β (which control the magnitudes of the modifications in R_S^A and R_G^A) while keeping the location parameters x_a and x_e as well as the parameters controlling the small- x behaviour fixed to the values quoted in Table 2. Minimization of χ^2 first with the freed sea quark parameters, then with the freed gluon parameters results in the wide bands shown by the dotted lines in Fig. 12. This demonstrates clearly how badly the nuclear sea quark and gluon modifications are constrained in the large- x region. Similar results have been presented before by the *HKN* group. Thus, as the error

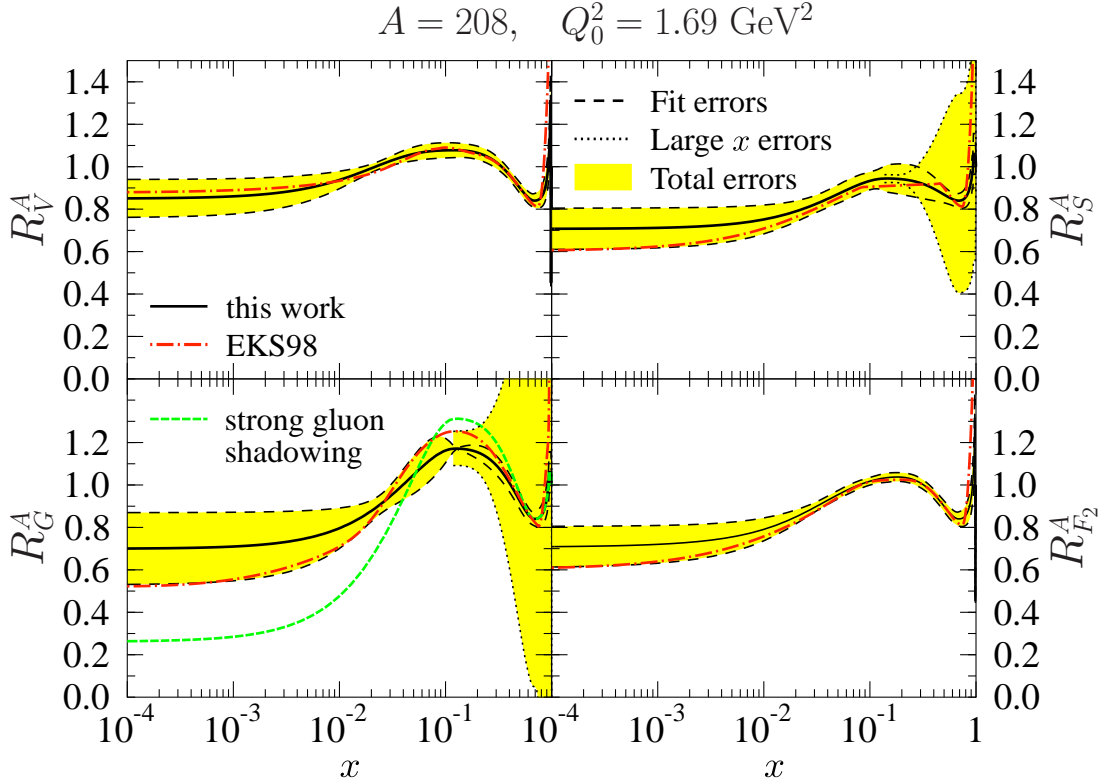


Figure 12: (Colour online) Fit errors at the initial scale $Q_0^2 = 1.69 \text{ GeV}^2$ for Lead, shown by the dashed lines. For large- x sea and gluon modifications the errors shown by the dotted lines were calculated separately, see the text. The shaded (yellow on-line) band is the total error estimate obtained, see the text. The corresponding *EKS98* results, evolved downwards from $Q_{0,EKS}^2 = 2.25 \text{ GeV}^2$, are shown by the dot-dashed (red) lines. An example of a stronger gluon shadowing is shown by dense-dashed (green) line.

estimates for the present analysis, we give the shaded (yellow on-line) bands of the small- x and large- x errors, denoting them by "total errors" in Fig. 12.

In Fig. 12 we also show the comparison with the *EKS98* modifications, evolved from a higher initial scale, $Q_{0,EKS}^2 = 2.25 \text{ GeV}^2$, down to the present one, $Q_0^2 = 1.69 \text{ GeV}^2$. Within the errors estimated, we can safely conclude that the old *EKS98* parametrization is fully consistent with the present χ^2 -minimization analysis. As discussed in the previous section, the fact that *EKS98* sea quarks and gluons lie somewhat below the results from this work, is mainly due to the different functional forms assumed for the fit functions at small values of x . We thus conclude that there is no need for releasing a new LO parametrization, since *EKS98* still works very well.

6 Stronger gluon shadowing?

Similarly to our earlier work *EKS98*, the present analysis suggests that the nuclear gluon modifications in the region $x \sim 0.02 - 0.04$ should be rather small, while the amounts of shadowing and thus antishadowing are much more weakly constrained. As the final task in this paper we discuss the possibility of a stronger gluon shadowing. Our main motivation for doing this is the inclusive charged-hadron data taken from D+Au collisions at RHIC by the BRAHMS collaboration [41], and the computation of the corresponding p_T spectra in Ref. [42] using the strong gluon shadowing suggested in Refs. [21, 43, 12]. These data are advocated as a hint that a parton saturation regime could have been reached at RHIC [44], so the degree of agreement with a DGLAP approach is of special interest.

We construct our strong gluon shadowing example by changing only the parameter y_a for the Carbon reference nucleus in R_G^A . Then, as seen in Fig. 12 the changes in the region $x \sim 0.02 - 0.04$ remain small but the amounts of antishadowing and (through momentum conservation) shadowing change. Increasing y_a from 1.071 to 1.2 deepens the saturation level of gluon shadowing in Lead considerably, from 0.7 to 0.26. At the same time, the goodness χ^2/N of the overall fit weakens only slightly, from 0.80 to 0.95, even if no χ^2 minimization was performed.

With the gluon shadowing much stronger than that of sea quarks, the $\log Q^2$ slopes of $R_{F_2}^A$ at small x are initially negative. At the same time, due to the stronger gluon antishadowing, the scale evolution of R_S^A near $x \sim 0.1$ is slightly speeded up. These effects can be verified in Fig. 13 (compare with Fig. 2). In fact, the latter effect is responsible for the deterioration of the goodness. We stress, however, that for this strong gluon shadowing example we have kept the quark sector as given in Table 2. After minimization, the changes in χ^2/N would become even smaller, demonstrating the fact that quite large changes in the gluon sector induce only small changes in the global χ^2 . This is interesting when compared with the results of de Sassot and Florian [9], who get considerably worse χ^2 values for stronger gluon shadowing. Apparently, the form of their fit is such that stronger gluon shadowing in small- x affects in the region $x \sim 0.01 - 0.1$ as well, thus changing the fit there.

In Fig. 14 we show the ratio R_{DAu} for minimum bias single hadron production, defined as

$$R_{DAu} = \frac{\frac{1}{A} \frac{d\sigma^{DAu}}{dp_T d\eta}}{\frac{d\sigma^{PP}}{dp_T d\eta}}, \quad (15)$$

where p_T and η are the hadronic transverse momentum and pseudorapidity, correspondingly. The BRAHMS data in the top panels are for $R_{DAu}(h^+ + h^-)$ and in the bottom panels for $R_{DAu}(h^-)$. The generic structure of the lowest order pQCD cross sections is given by

$$\sigma^{AB \rightarrow h+X} = \sum_{ijkl} f_i^A(x_1, Q) \otimes f_j^B(x_2, Q) \otimes \sigma^{i+j \rightarrow k+l} \otimes D_{k \rightarrow h+X}(z, Q_f), \quad (16)$$

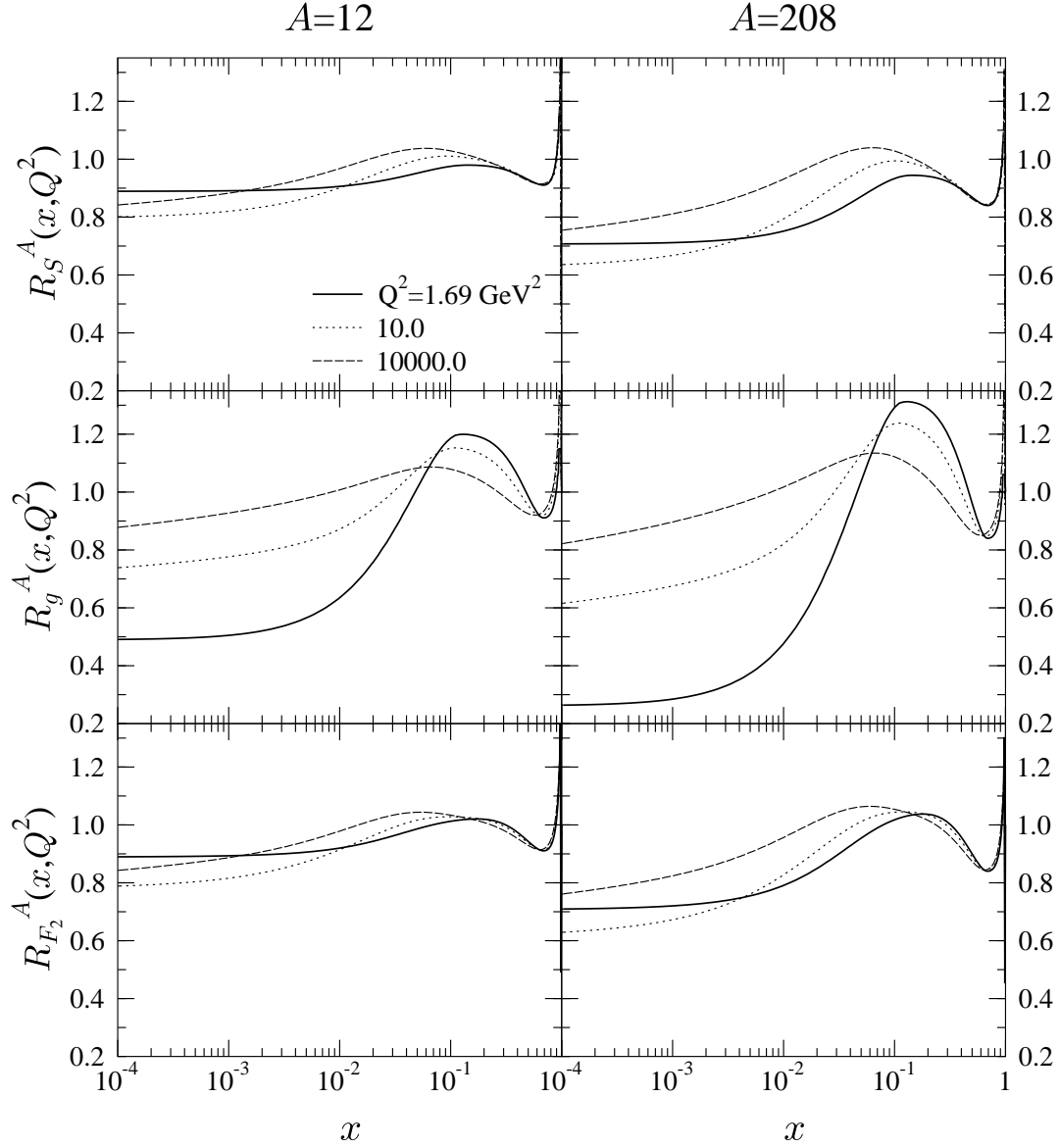


Figure 13: Scale evolution of the ratios R_S^A , R_G^A and $R_{F_2}^A$ for Carbon and Lead in the case of the strong gluon shadowing example considered in Fig. 12. Notice the initial negative $\log Q^2$ slopes of R_S^A and hence also $R_{F_2}^A$ at small values of x .

where h is the hadron type, k labels the parton type, $AB = \text{DAu}, \text{pp}$ and $D_{k \rightarrow h+X}(z, Q_f)$ are the fragmentation functions at a fractional energy $z = E_h/E_k$ and a factorization scale Q_f . Detailed formulation of the computation can be found e.g. in [45]. Here we choose Q as the transverse momentum of the parton and Q_f as the transverse momentum of the hadron. We use the KKP fragmentation functions [46] and the CTEQ6L1 free proton PDFs. We do not make attempt to correct for the fact that the KKP fragmentation functions correspond to the average $h^+ + h^-$, even though the forward-rapidity data is for negative hadrons only.

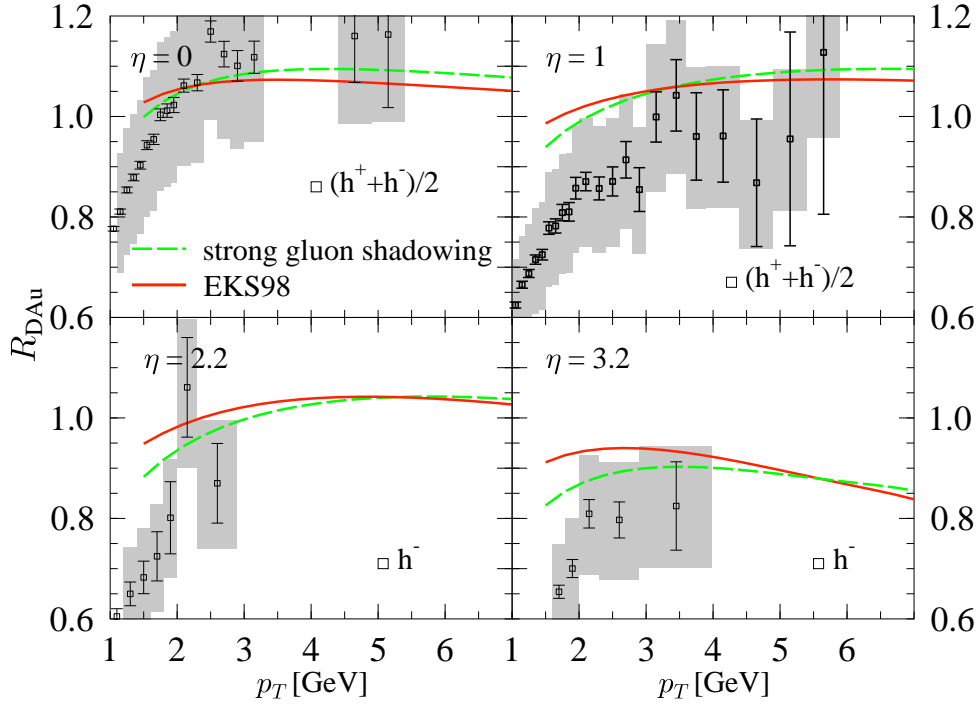


Figure 14: (Colour online) Minimum bias inclusive hadron production cross sections in d+Au collisions divided by that in p+p collisions at $\sqrt{s_{NN}} = 200$ GeV at RHIC. The ratio R_{DAu} is shown as a function of hadrons transverse momentum at four different pseudorapidities. The BRAHMS data [41] are shown with the statistical error bars and the shaded systematic error limits. A pQCD calculation for $h^+ + h^-$ production with the *EKS98* nuclear modifications and KKP fragmentation functions is shown by the solid lines (red) and that with the strong gluon shadowing by the dashed lines (green).

At small pseudorapidities, where both quark and gluon-initiated processes are important, the stronger gluon antishadowing induces only a small correction to R_{DAu} but in a manner that the overall shape of the computed R_{DAu} agrees better with the BRAHMS data. At large pseudorapidities, corresponding to smaller x_2 , gluons become dominant. As discussed in [45], hadron production at, say, 1.5 GeV is biased to

partons at $p_T \sim 3$ GeV. Since $x_2 = \frac{p_T}{\sqrt{s}}(e^{-\eta} + e^{-y_2})$, small values of x_2 of the order 0.001, start to play a role at $\eta = 3$. Integration over y_2 (or x_2) however, smears the effects of the nuclear modifications which is why we do not see a larger change in R_{DAu} with the stronger gluon shadowing example considered. As shown in Ref. [42], even more dramatic small- x behaviour of gluons, such as suggested in [21, 43, 12], would obviously be needed to account for the BRAHMS data. Whether gluons with such shadowing, supplemented perhaps with stronger shadowing for the sea quarks as well, would maintain the good global fit to the DIS and DY data now obtained, remains to be seen. At the same time, dependence of the fragmentation functions on the hadron charge (negatives instead of the average $h^+ + h^-$), should be studied in more detail within a consistent DGLAP framework.

Due to the double integrations in computing the cross sections in Eq. 16, inclusion of the RHIC data for R_{DAu} in the global analysis is beyond the scope of the present paper. As further data constraints are absolutely necessary for pinning down the nuclear gluons, these data, in spite of their relatively large systematic errors, motivate us to do this in future.

7 Summary

In this study we have performed a global leading-order DGLAP analysis of the nPDFs using the *EKS98* framework introduced in [5, 6]. Motivated by our previous work, we have introduced a piece-wise parametrization for the nuclear effects in the PDFs. Originally, the fit functions contained altogether 42 parameters. With the help of momentum and baryon number conservation and the experience from *EKS98*, we reduce the number of relevant fit parameters down to 16. A best fit to the nuclear DIS and DY data was searched for this set of parameters through automated minimization of χ^2 using the Minuit program [37]. As a result, a very good fit to the $N = 514$ data points at $Q^2 \geq 1.69$ GeV² was found, giving $\chi^2/N = 0.789$ (or $\chi^2/\text{d.o.f.} = 0.82$). No essential improvement over *EKS98* was found, however, as the *EKS98* modifications lead to an equally good fit quality, $\chi^2/N = 0.809$ (for $N = 479$ datapoints at $Q^2 \geq Q_{0,\text{EKS98}}^2$).

Relative to the old *EKS98*, the present analysis suggests slightly less shadowing for the gluons and sea quarks. This, however, is merely due to the different forms of the fit functions adopted in the region where no stringent constraints from the data are available. We also compared the obtained nuclear effects to those obtained by other global analyses, *HKM*, *HKN*, and *nDS*. The valence quark modifications do not deviate much from one set to another but the smallest- x and large- x modifications of gluons and sea quarks differ in a major way. This reflects the fact that especially the nuclear gluons are badly constrained in these regions.

To quantify the uncertainties in our analysis, we obtained the error estimates by using the Hessian method based on the information given by Minuit. The error estimates obtained also nicely further confirm the validity of *EKS98*, as it is shown to be fully consistent with the present analysis.

To get a hold on the uncertainties in the large- x regions of gluons and sea quarks, we computed the large- x errors separately. These, considered together with the small- x errors on the best fit confirm the conclusions from the comparison between different analyses: the valence quark distributions are relatively well, and independently from the fit-function form, constrained over the whole x region. For the sea quarks, the large- x ($x \gtrsim 0.3$) errors become very large, and for the small- x behaviour clearly depends on the fit function form. For gluons, our analysis shows that presently one can to some extent constrain the gluons in the region $x \sim 0.02 - 0.04$ but hardly at all in the large- x region, and only in a fit-function-dependent manner at small x through momentum conservation. We also note that the relatively small error estimate obtained at $x \sim 0.02 - 0.04$ for gluons may depend somewhat on the framework chosen, as the gluon fit parameters were drifting to the limits imposed. This obviously leaves room for further improvements in the future. An obvious further improvement of the present analysis is its extension to NLO.

As the DIS and DY data are not able to stringently pin down the gluon modifications, further constraints are obviously needed. In thinking of possible additional data sets to be included in the global analysis in the future, we considered an example of a stronger gluon shadowing without doing a χ^2 minimization. First, we showed that quite large variations in the gluon modifications can be absorbed in the quark sector and thus hidden by the good χ^2 values obtained. Then, motivated by Ref. [42], we computed the nuclear modification ratio R_{DAu} of inclusive hadron production in d+Au relative to that in pp, using both the *EKS98* modifications and the strong gluon shadowing example. Comparisons against the BRAHMS data [41] here and in Ref. [42] lend support to more shadowed gluons than in the present *EKS98* framework. At RHIC, the d+Au data is evidently very valuable for getting further constraints for nuclear gluons in particular. This in turn demonstrates the importance of running a parallel p+Pb program at the LHC, where pQCD factorization and nPDFs could be tested further in a wide range of x and Q^2 .

Acknowledgements

CAS is supported by the 6th Framework Programme of the European Community under the Marie Curie contract MEIF-CT-2005-024624. We thank the Academy of Finland, Projects 73101, 80385, 206024 and 115262 for financial support.

References

- [1] A. D. Martin, R. G. Roberts, W. J. Stirling and R. S. Thorne, Eur. Phys. J. C **35** (2004) 325 [arXiv:hep-ph/0308087].
- [2] J. Pumplin, D. R. Stump, J. Huston, H. L. Lai, P. Nadolsky and W. K. Tung, JHEP **0207** (2002) 012 [arXiv:hep-ph/0201195].

- [3] D. Stump, J. Huston, J. Pumplin, W. K. Tung, H. L. Lai, S. Kuhlmann and J. F. Owens, JHEP **0310**, 046 (2003) [arXiv:hep-ph/0303013].
- [4] Y. L. Dokshitzer, Perturbation Theory In Quantum Sov. Phys. JETP **46** (1977) 641 [Zh. Eksp. Teor. Fiz. **73** (1977) 1216]; V. N. Gribov and L. N. Lipatov, Yad. Fiz. **15** (1972) 781 [Sov. J. Nucl. Phys. **15** (1972) 438]; V. N. Gribov and L. N. Lipatov, Yad. Fiz. **15** (1972) 1218 [Sov. J. Nucl. Phys. **15** (1972) 675]; G. Altarelli and G. Parisi, Nucl. Phys. B **126** (1977) 298.
- [5] K. J. Eskola, V. J. Kolhinen and P. V. Ruuskanen, Nucl. Phys. B **535** (1998) 351 [arXiv:hep-ph/9802350].
- [6] K. J. Eskola, V. J. Kolhinen and C. A. Salgado, Eur. Phys. J. C **9** (1999) 61 [arXiv:hep-ph/9807297].
- [7] M. Hirai, S. Kumano and M. Miyama, Phys. Rev. D **64** (2001) 034003 [arXiv:hep-ph/0103208].
- [8] M. Hirai, S. Kumano and T. H. Nagai, Phys. Rev. C **70** (2004) 044905 [arXiv:hep-ph/0404093].
- [9] D. de Florian and R. Sassot, Phys. Rev. D **69** (2004) 074028 [arXiv:hep-ph/0311227].
- [10] N. Armesto, J. Phys. G **32** (2006) R367 [arXiv:hep-ph/0604108].
- [11] M. Arneodo, Phys. Rept. **240** (1994) 301.
- [12] A. Accardi *et al.*, CERN Yellow Report for Hard Probes at the LHC, “Hard probes in heavy ion collisions at the LHC: PDFs, shadowing and p A collisions,” arXiv:hep-ph/0308248; see Sec. 4.
- [13] M. Arneodo *et al.* [New Muon Collaboration], Nucl. Phys. B **481** (1996) 23.
- [14] J. w. Qiu, Nucl. Phys. B **291** (1987) 746.
- [15] L. L. Frankfurt, M. I. Strikman and S. Liuti, Phys. Rev. Lett. **65** (1990) 1725.
- [16] K. J. Eskola, Nucl. Phys. B **400** (1993) 240.
- [17] S. Kumano, Phys. Rev. C **48** (1993) 2016 [arXiv:hep-ph/9303306].
- [18] S. Kumano, Phys. Rev. C **50** (1994) 1247 [arXiv:hep-ph/9402321].
- [19] D. Indumathi and W. Zhu, Z. Phys. C **74** (1997) 119 [arXiv:hep-ph/9605417].
- [20] D. Indumathi, Z. Phys. C **76** (1997) 91 [arXiv:hep-ph/9609361].

- [21] L. Frankfurt, V. Guzey and M. Strikman, Phys. Rev. D **71** (2005) 054001 [arXiv:hep-ph/0303022].
- [22] <http://www.phys.psu.edu/~cteq/>
- [23] K. J. Eskola and H. Paukkunen, JHEP **0606** (2006) 008 [arXiv:hep-ph/0603155].
- [24] D. M. Alde *et al.*, Phys. Rev. Lett. **64** (1990) 2479.
- [25] J. Gomez *et al.*, Phys. Rev. D **49** (1994) 4348.
- [26] M. R. Adams *et al.* [E665 Collaboration], Z. Phys. C **67** (1995) 403 [arXiv:hep-ex/9505006].
- [27] P. Amaudruz *et al.* [New Muon Collaboration], Nucl. Phys. B **441** (1995) 3 [arXiv:hep-ph/9503291].
- [28] M. Arneodo *et al.* [New Muon Collaboration.], Nucl. Phys. B **441** (1995) 12 [arXiv:hep-ex/9504002].
- [29] M. Arneodo *et al.* [New Muon Collaboration], Nucl. Phys. B **481** (1996) 3.
- [30] M. A. Vasilev *et al.* [FNAL E866 Collaboration], Phys. Rev. Lett. **83** (1999) 2304 [arXiv:hep-ex/9906010].
- [31] Jan Czyzewski, K.J. Eskola and J. Qiu, at the III International Workshop on Hard Probes of Dense Matter, ECT., Trento, June 1995.
- [32] K. J. Eskola, H. Honkanen, V. J. Kolhinen and C. A. Salgado, Phys. Lett. B **532** (2002) 222 [arXiv:hep-ph/0201256].
- [33] H. Honkanen, PhD Thesis, Research Report 1/2005, University of Jyväskylä, Department of Physics, January 2005; see Fig. 2.3.
- [34] J. w. Qiu and I. Vitev, Phys. Rev. Lett. **93**, 262301 (2004) [arXiv:hep-ph/0309094].
- [35] L. V. Gribov, E. M. Levin and M. G. Ryskin, Phys. Rept. 100 (1983) 1; A. H. Mueller and J. Qiu, Nucl. Phys. B 268 (1986) 427.
- [36] K. Prytz, Phys. Lett. B **311** (1993) 286.
- [37] F. James, MINUIT Function Minimization and Error Analysis, Reference Manual Version 94.1. CERN Program Library Long Writeup D506 (Aug 1998).
- [38] J. Pumplin *et al.*, Phys. Rev. D **65** (2002) 014013 [arXiv:hep-ph/0101032].
- [39] M. Hirai, S. Kumano and N. Saito [Asymmetry Analysis Collaboration], Phys. Rev. D **69** (2004) 054021 [arXiv:hep-ph/0312112].

- [40] T. Gousset and H. J. Pirner, Phys. Lett. B **375** (1996) 349 [arXiv:hep-ph/9601242].
- [41] I. Arsene *et al.* [BRAHMS Collaboration], Phys. Rev. Lett. **93** (2004) 242303 [arXiv:nucl-ex/0403005].
- [42] R. Vogt, Phys. Rev. C **70** (2004) 064902.
- [43] L. Frankfurt, V. Guzey, M. McDermott and M. Strikman, JHEP **0202** (2002) 027 [arXiv:hep-ph/0201230].
- [44] R. Baier, A. Kovner and U. A. Wiedemann, Phys. Rev. D **68**, 054009 (2003);
D. Kharzeev, Y. V. Kovchegov and K. Tuchin, Phys. Rev. D **68** (2003) 094013;
J. L. Albacete, N. Armesto, A. Kovner, C. A. Salgado and U. A. Wiedemann,
Phys. Rev. Lett. **92**, 082001 (2004).
- [45] K. J. Eskola and H. Honkanen, Nucl. Phys. A **713**, 167 (2003) [arXiv:hep-ph/0205048].
- [46] B. A. Kniehl, G. Kramer and B. Potter, Nucl. Phys. B **582** (2000) 514 [arXiv:hep-ph/0010289].